Molecular Therapy
Original Article

PARP1 modulates *METTL3* promoter chromatin accessibility and associated LPAR5 RNA m^{6}A methylation to control cancer cell radiosensitivity

Xiaoya Sun,[1,2,5] Chenjun Bai,[2,5] Haozheng Li,[1,2] Dafei Xie,[2] Shi Chen,[1,2] Yang Han,[2] Jinhua Luo,[2,3] Yang Li,[4] Yumeng Ye,[4] Jin Jia,[1,2] Xin Huang,[2] Hua Guan,[2] Dingxin Long,[1] Ruixue Huang,[3] Shanshan Gao,[2] and Ping-Kun Zhou[1,2]

[1]School of Public Health, Hengyang Medical School, University of South China, Hengyang, Hunan 421001, P.R. China; [2]Department of Radiation Biology, Beijing Key Laboratory for Radiobiology, Beijing Institute of Radiation Medicine, Beijing 100850, P.R. China; [3]Department of Occupational and Environmental Health, Xiangya School of Public Health, Central South University, Changsha, Hunan 410078, P.R. China; [4]Department of Experimental Pathology, Beijing Institute of Radiation Medicine, Beijing 100850, P.R. China

Chromatin remodeling and N^6-methyladenosine (m^{6}A) modification are two critical layers in controlling gene expression and DNA damage signaling in most eukaryotic bioprocesses. Here, we report that poly(ADP-ribose) polymerase 1 (PARP1) controls the chromatin accessibility of *METTL3* to regulate its transcription and subsequent m^{6}A methylation of poly(A)$^+$ RNA in response to DNA damage induced by radiation. The transcription factors nuclear factor I-C (NFIC) and TATA binding protein (TBP) are dependent on PARP1 to access the *METTL3* promoter to activate *METTL3* transcription. Upon irradiation or PARP1 inhibitor treatment, PARP1 disassociated from *METTL3* promoter chromatin, which resulted in attenuated accessibility of NFIC and TBP and, consequently, suppressed METTL3 expression and RNA m^{6}A methylation. Lysophosphatidic Acid Receptor 5 (LPAR5) mRNA was identified as a target of METTL3, and m^{6}A methylation was located at A1881. The level of m^{6}A methylation of LPAR5 significantly decreased, along with METTL3 depression, in cells after irradiation or PARP1 inhibition. Mutation of the LPAR5 A1881 locus in its 3′ UTR results in loss of m^{6}A methylation and, consequently, decreased stability of LPAR5 mRNA. METTL3-targeted small-molecule inhibitors depress murine xenograft tumor growth and exhibit a synergistic effect with radiotherapy *in vivo*. These findings advance our comprehensive understanding of PARP-related biological roles, which may have implications for developing valuable therapeutic strategies for PARP1 inhibitors in oncology.

INTRODUCTION

Chromatin remodeling is an early critical molecular event in the cellular response to nuclear DNA damage, which controls access to genomic DNA and is strongly associated with processing of DNA repair and gene expression regulation.[1,2] The poly(ADP-ribose) (PAR) polymerase (PARP1) is an important nuclear protein with multiple functions in maintenance of genome integrity, regulation of gene transcription, and metabolism as well as a series of signal transduction processes associated with cell death, aging, cancer sensitivity to chemo/radiotherapy, etc.[3,4] As an important chromatin-binding nucleoprotein, PARP1 functions in chromatin remodeling; e.g., it works together in multiple ways with the ATPase amplified in liver cancer 1 (ALC1), the only SNF2-family chromatin remodeling enzyme with a PAR-binding macrodomain.[5] With its multifaceted actions in chromatin remodeling, gene expression, DNA damage response, and repair, PARP1 plays a critical role in cell fate determination and maintenance of genomic stability.[6–8] When DNA damage occurs, the interaction between PARP1 protein and damaged DNA causes PARP1 to be temporarily activated, triggering the DNA repair pathway, and then PARP1 loses its ability to interact with DNA and is released from chromatin. Thus, PARP inhibitors are widely designed and developed as a new class of chemotherapy agents. One of the mechanistic theories is based on the genetic concept of synthetic lethality, which refers to a situation where co-occurrence of multiple gene mutations results in cell death, aiming to target cancers with breast cancer (BRCA) mutations and homologous recombination defects.[3,9,10] To date, there are at least four PARP inhibitors with US Food and Drug Administration (FDA) regulatory approval for treatment of several types of cancer with BRCA-associated 1/2 (BRCA1/2)

Received 28 February 2023; accepted 20 July 2023;
https://doi.org/10.1016/j.ymthe.2023.07.018.

[5]These authors contributed equally

Correspondence: Ping-Kun Zhou, Department of Radiation Biology, Beijing Key Laboratory for Radiobiology, Beijing Institute of Radiation Medicine, Beijing 100850, P.R. China.
E-mail: zhoupk@bmi.ac.cn
Correspondence: Shanshan Gao, Department of Radiation Biology, Beijing Key Laboratory for Radiobiology, Beijing Institute of Radiation Medicine, Beijing 100850, P.R. China.
E-mail: gaoshanbprc@163.com
Correspondence: Ruixue Huang, Department of Occupational and Environmental Health, Xiangya School of Public Health, Central South University, Changsha, Hunan 410078, P.R. China.
E-mail: huangruixue@csu.edu.cn

mutations.[3] This kind of anticancer drug acts as a direct inhibitor of PARylation enzyme activity or "traps" PARP in a chromatin-bound state,[3,11] which is closely related to the activities of gene transcription and DNA repair.

Radiotherapy is one of the conventional effective therapies available for tumor treatment. Approximately 50%–60% of cancer patients receive radiotherapy during the course of the disease. Radiotherapy is sometimes used alone, but most times it is applied in combination with other therapy strategies, such as surgery, chemotherapy,[12,13] immunotherapy,[14] and targeted radiosensitizers.[15,16] A combination of PARP inhibitors with radiotherapy is considered an important and effective treatment option for various cancers.[17–19] It is an important task to identify the cellular radiosensitivity-modifying genes and regulatory networksfor developing precise, targeted countermeasures that can not only improve the effectiveness of cancer radiotherapy but also decrease radiotoxicity to normal tissues. Overall, chromatin structure nuclear architecture critically influences the dynamics and extent of gene transcription, DNA damage repair, and, thus, the cellular response to radiation.[20] PARP1 is undoubtedly an important target and functioning molecule to determine cell fate after radiation exposure, while little is known about the downstream targets, mediated signaling pathways, and associated cellular outcomes affected by its modulation of chromatin remodeling.

RNA m^{6}A modification is another critical layer of controlling gene expression downstream of transcription in various bioprocesses in eukaryotes, such as cell differentiation, cell division, immunity, DNA repair and fate, tumor development, and cancer therapy implications, by regulating RNA splicing, nuclear transfer, translation regulation, and degradation.[21–23] The sequence of the m^{6}A modification site on mRNA is highly conserved, mainly occurring on the adenine of RRACH (R = G, A; H = A, C, or U).[24] The m6A balance in cells is regulated by m^{6}A writers, erasers, and reader proteins. m^{6}A writers (i.e., methyltransferases [MTases]) include MTase-like 3 (METTL3), METTL14, Wilms tumor 1-associated protein (WTAP), KIAA1429, METTL16, RBM15, and ZC3H13.[25] METTL3, METTL14, and WTAP form the complex of the critical m^{6}A writer, among which METTL3 is the catalytic core subunit, and METTL14 serves as an RNA-binding platform.[26–28] The METTL14 C-extension is rich in RGG/RG motifs and is important for RNA binding of the entire METTL3/METTL14 complex.[26] WTAP functions as an m^{6}A regulator to relocate the ternary MTase complex to nuclear speckles, which are rich in mRNA substrates.[28] Knockdown of METTL3, METTL14, and WTAP decreases the m^{6}A level in poly(A)$^+$ RNA by ~30%, ~40%, and 50% in HeLa cells.[29] Demethylases act as m^{6}A erasers and include fat mass and obesity-associated protein (FTO)[30] and α-ketoglutarate-dependent dioxygenase alkB homolog 5 (ALKBH5).[31] The m^{6}A readers recognize and bind the m^{6}A motif, playing a critical role in processing of m^{6}A-containing RNAs in the nucleus and cytoplasm. YT521-B homology (YTH) domain-containing proteins represent the major class of m^{6}A readers, which include YTH domain-containing protein 1 (YTHDC1), YTHDC2, and the family of YTH domain family (YTHDF) proteins.[25,32,33] YTHDC1 is a nuclear m^{6}A reader, YTHDC2 can be nuclear and cytosolic, and YTHDF family members are cytosolic. Some RNA-binding proteins can be recruited by m^{6}A indirectly, so-called indirect m^{6}A readers, such as heterogeneous nuclear ribonucleoprotein C (HNRNPC), HNRNPG, and HNRNPA2B1.[34] m^{6}A modification and the related enzymes and proteins have been demonstrated to be involved in a series of vital processes responding to various stimuli and stresses, such as the Reactive oxygen species (ROS)-induced DNA damage response,[35] UV-induced DNA damage response,[36] and integrated stress response (ISR).[37] Emerging evidence indicates that dynamic changes in m^{6}A modification provide a new direction for formulation of tumor radiotherapy and chemotherapy strategies.[38] METTL3 is the predominantly catalytic enzyme of the methyltransferase (MTase) complex, and METTL3 is implied to become a new target for tumor radiotherapy and chemotherapy sensitization.[39] METTL3 mediates m^{6}A methylation of circCUX1 and stabilizes its expression, thereby developing tolerance to radiotherapy.[40] METTL3-silenced glioma stem-like cells (GSCs) show enhanced sensitivity to γ irradiation and reduced DNA repair.[41]

In the present study, we sought to investigate the interplay of m^{6}A modification and the cellular response to ionizing radiation. We found that METTL3 expression and its mediated m^{6}A modification decreased significantly in A549 and HeLa cells after γ-ray exposure or PARP1 inactivation. Upon irradiation, PARP1 dissociated from the *METTL3* promoter region, which led to decreased accessibility of *METTL3* promoter chromatin for transcription factors. We also identified LARP5 as a target of METTL3-mediated m^{6}A modification. Radiation and PARP1 inhibitors suppress METTL3-mediated m^{6}A modification, which prompts radiation-induced apoptosis at least partially via targeted LPAR5 signaling. A small-molecule inhibitor of METTL3 was further confirmed to markedly suppress tumor growth and exhibited an additive inhibitory effect with radiation *in vivo*. Taken together, we revealed a new aspect of PARP1 function, coupling chromatin remodeling and m^{6}A modification regulation, which provides favorable knowledge for developing and precisely applying PARP inhibitors for cancer therapy as well as improving the effectiveness of radiotherapy in cancer treatment.

RESULTS

Radiation depresses METTL3 expression and its associated m^{6}A methylation of poly(A)$^+$ RNAs

Previous reports have demonstrated that RNA m^{6}A modification is increased and involved in DNA damage responses (DDRs) following UV irradiation[36,42] but not exposure to 10 Gy γ-ray ionizing radiation (IR).[36] However, the pattern of m^{6}A-modified RNAs, the underlying regulatory mechanism, and their roles in the cellular response to IR remain unclear. To identify the role of m^{6}A modification in IR-induced DDR *in vitro*, tumor cells were irradiated with 4 Gy of γ-ray radiation. The overall m^{6}A modification of RNAs was quantitatively detected by poly(A)$^+$ RNA m^{6}A quantification, as described under Materials and methods section. The results indicate that the total level of m^{6}A modification was significantly suppressed 2 h after irradiation and until 12 h after IR in HeLa (Figure 1A) and A549

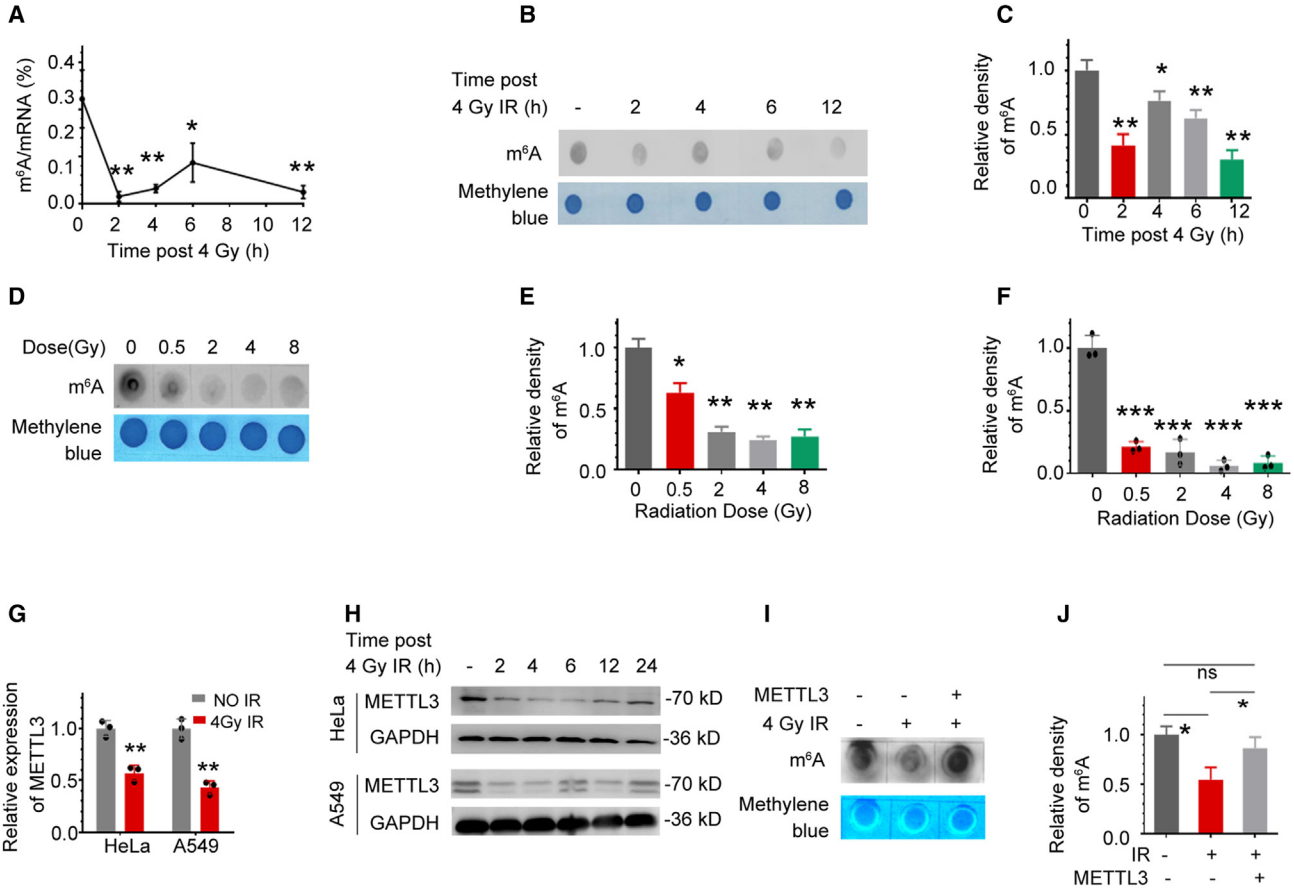

Figure 1. Decreased m^{6}A methylation of poly(A)$^+$ RNA upon exposure to IR

(A) The m^{6}A modification level of total poly(A)$^+$ RNA in HeLa cells was detected by RNA methylation quantification (colorimetric assay) at given times after 4-Gy γ-ray irradiation. (B and C) m^{6}A methylation level of total poly(A)$^+$ RNA in HeLa cells was detected by m^{6}A dot blot assay (B) and the corresponding quantification (C) at given times after 4-Gy γ-ray irradiation. (D and E) The m^{6}A methylation level of total poly(A)$^+$ RNA in HeLa cells was detected 2 h after different doses of γ-ray irradiation by m^{6}A dot blot assay (D) and corresponding quantification (E). (F) The m^{6}A methylation level of total poly(A)$^+$ RNA in HeLa cells was detected 2 h after doses of γ-ray irradiation by RNA methylation quantification (colorimetric assay). (G and H) The expression of METTL3 was detected by qPCR 2 h after 4-Gy irradiation (G) or western blot analysis (H) at given times after 4-Gy γ-ray irradiation. (I and J) Effect of transfecting/overexpressing exogenous METTL3 vectors on the change in m^{6}A level of total poly(A)$^+$ RNA at 2 h after 4-Gy irradiation was detected by m^{6}A dot blot assay (I) and corresponding quantification (J) in HeLa cells. All data represent the mean ± SD from three independent experiments. Compared with the control, *$p < 0.05$, **$p < 0.01$.

(Figure S1A) cells. Dot blot assays also showed that m^{6}A RNA was decreased from at least 2 h after γ-ray irradiation in HeLa (Figures 1B and 1C) and A549 cells (Figures S1B and S1C). A dose-dependent decrease in m^{6}A RNA methylation was also observed from 0.5-Gy dose of irradiation (Figures 1D–1F).

The m^{6}A MTase complex is composed of METTL3, METTL14, WTAP, KIAA1429, METTL16, RBM15, and ZC3H13. To identify how m^{6}A was repressed by IR, the expression of MTases (m^{6}A writers), demethylases (m^{6}A erasers), and other related binding proteins (readers) was detected using quantitative real-time PCR after irradiation (Figure S2). We found that the expression of METTL3, the core enzyme of m^{6}A MTase, was significantly repressed at the mRNA and protein levels (Figures 1G, 1H, and S11A), which is consistent with the alteration of overall m^{6}A methylation levels after IR. To confirm whether inhibition of overall m^{6}A methylation is related to repression of METTL3 expression, a dot blot assay was performed with specific anti-m^{6}A antibodies after IR in HeLa cells overexpressing METTL3. The results showed that IR-induced m^{6}A repression was rescued after overexpressing exogenous METTL3 (Figures 1I and 1J). These results imply that METTL3 at least partially mediates IR-induced repression of m^{6}A modification.

PARP1-mediated activation of *METTL3* transcription and depression by radiation

To identify the mechanism of IR-induced METTL3 repression, we first detected the stability of METTL3 mRNA after IR. The half-life of METTL3 RNA did not change significantly after 4-Gy IR (Figure S3A). Then, we found that irradiation and knockdown of PARP1 inhibited the promoter activity of *METTL3*, as detected by

luciferase reporter experiments (Figures S3B and S3C). We then selected two known transcriptional activators of *METTL3*, TATA binding protein (TBP)[43] and nuclear factor I-C (NFIC)[44], to identify whether IR repressed expression of TBP and/or NFIC. Expression of TBP and NFIC was stable after irradiation (Figure S3D). Therefore, we identified whether IR affects binding of TBP and NFIC to the *METTL3* promoter. Chromatin immunoprecipitation (ChIP) assays indicated that the occupancy of TBP and NFIC proteins was inhibited after IR (Figure 2A). To identify how binding of TBP and NFIC with the *METTL3* promoter was inhibited, protein pull-down and subsequent mass spectrometry (MS) assays were performed after the cell nucleoprotein was incubated with the biotin-labeled *METTL3* promoter fragment. Several proteins were found to bind with the *METTL3* promoter fragment (Figures S3E and S3F), which included decreased binding of PARP1 after IR. However, PARP1 expression was not changed after 4-Gy irradiation (Figure S3G). To confirm repression of PARP1 binding with the *METT*3 promoter, a ChIP assay was performed with a specific anti-PARP1 antibody. We confirmed that the PARP1 protein binds to the *METTL3* promoter, which was inhibited by IR (Figure 2B). Our protein truncation analysis revealed that the *METTL3* promoter is associated with the DBD (DNA binding domain) of PARP1, and interaction between NFIC and the *METTL3* promoter was also observed (Figures 2C and S3H). To confirm regulation of METTL3 expression by PARP1, METTL3 mRNA and protein expression were detected in HeLa cells treated for 10 h with 10 μM PARP1 inhibitors (PARPis) NMS-P118 and olaparib or in HeLa cells with depressed PARP1 by its specific small interfering RNAs (siRNAs) (Figure S3I). We found that the mRNA and protein levels of METTL3 were reduced by PARPi (Figures 2D, 2E, and S11B) and PARP1 depression (Figures 2F, 2G, and S11C). The decreased METTL3 can be rescued by expressing siRNA-resistant PARP1. To understand whether downregulation of METTL3 by radiation is mediated through any other signaling in addition to the PARP1 pathway, the cells were pretreated with a PARPi before irradiation. It can be seen that there is no additional depression on METTL3 by radiation in the cells treated with 10 μm PARPi for 6 hours, suggesting no combined inhibition effect between PARPi and radiation on METTL3 expression (Figures 2H, 2I, and S11D). Likewise, radiation barely further inhibited METTL3 expression in PARP1 knockdown cells (Figures 2J, 2K, and S11E). All of these results indicate that *METTL3* is a PARP1-responsive gene. IR potentially inhibited binding of PARP1 protein to the *METTL3* promoter.

PARP1 modulates accessibility of *METTL3* promoter chromatin to impact its transcription

Given that PARP1 has the ability to bind to nucleosomes and even undamaged DNA to organize the chromatin structure of target genes[45–48] and that PARP1 binds to the *METTL3* promoter, as shown above, we explored whether PARP1 controls the accessibility of *METTL3* promoter chromatin. The chromatin of the *METTL3* promoter region is inaccessible and cannot be digested by micrococcal nuclease (MNase protection) when it is tightly compacted. The integrity of *METTL3* promoter DNA around the transcription start sites (TSSs; approximately −400 to +400 bp) was detected by quantitative real-time PCR in cell chromatin mixtures digested with MNase. Significantly increased protection against MNase digestion in the TSS of *METTL3* was detected after IR (Figure 3A). This protective effect was also detected in cells after PARPi treatment (Figure 3B). These results indicate that PARP1 functions in regulating the openness of METTL3 promoter chromatin.

To identify whether PARP1 controls access of the transcription factors NFIC and TBP to the *METTL3* promoter region, ChIP assays were performed with specific anti-NFIC or TBP antibodies. The results showed that binding of TBP or NFIC to the *METTL3* promoter was inhibited by the PARPi (Figure 3C). To exclude the possibility that TBP or NFIC mediates PARP1-regulated *METTL3* transcription, TBP and NFIC mRNA expression was detected in cells with stable si-PARP1. The results showed that there was no change in TBP and NFIC mRNA expression after siRNA-depressed PARP1 (Figure S3J). Consistent with this, *METTL3* is a PARP1-responsive gene. *METTL3* expression was synergistically suppressed in cells with siRNA-silenced TBP and/or NFIC (Figures 3D, 3E, S11F, S3K, and S3L) in combination with PARP1 silencing. However, PARP1-activated *METTL3* transcription is NFIC or TBP dependent. Transcription of *METTL3* was activated after PARP1 overexpression, and this activation was undetectable after NFIC and TBP silencing (Figures 3F, 3G, and S11G). Furthermore, overexpression of PARP1 rescued IR-induced *METTL3* repression. NFIC and/or TBP silencing abrogated the resecue effect of overexpressed PARP1 on IR-induced *METTL3* repression (Figures 3H, 3I, and S11H). All of these results indicate that PARP1-regulated *METTL3* transcription is NFIC and TBP dependent. PARP1 controls the accessibility of *METTL3* promoter chromatin to regulate NFIC and TBP binding to the *METTL3* promoter and activation of *METTL3* transcription.

METTL3 mediates PARP1-regulated m^{6}A methylation

Given that PAPR1 regulates *METTL3* transcription, we detected the role of PARP1 in m^{6}A methylation. Dot blot assays with specific m^{6}A antibodies indicated that m^{6}A methylation was dramatically decreased after PARP1 silencing (Figures 4A and 4B), which is similar to METTL3 silencing (Figures S3M–S3O). However, m^{6}A methylation was not synergistically repressed after METTL3 and PARP1 silencing (Figures 4C and 4D). Consistent with this, the m^{6}A modification was repressed in cells after irradiation or PARPi treatment, and there was no synergistic repressive effect of radiation and PARPi (Figures 4E and 4F). METTL3 is required for PARP1 overexpression-induced upregulation of m^{6}A modification in a dose-dependent manner (Figures 4G and 4H).

Transcriptome-wide m^{6}A sequencing (m^{6}A-seq) and RNA sequencing (RNA-seq) assays to identify potential m^{6}A-modified targets in response to IR

To identify the downstream m^{6}A-modified targets/mRNAs after IR, transcriptome-wide m^{6}A-seq, and RNA-seq assays were performed after IR in HeLa cells. Time points and radiation doses were selected based on the highest sensitivity of m^{6}A methylation in HeLa cells,

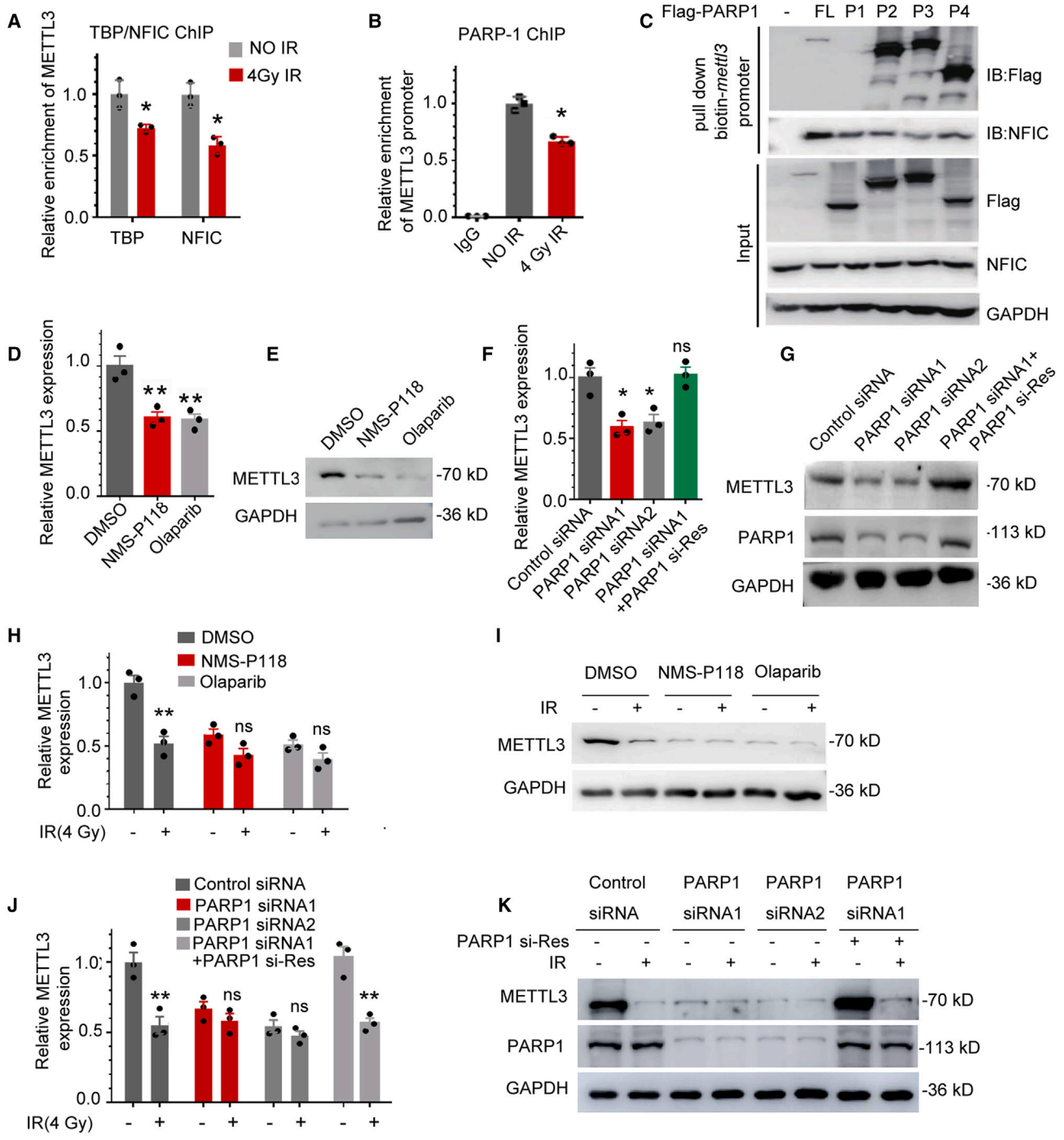

Figure 2. Suppression of METTL3 expression by irradiation and PARP1 inhibition

(A) Decreased binding of the transcription factors NFIC and TBP to the *METTL3* promoter after 4-Gy irradiation, as detected by ChIP-qPCR assay. (B) Confirmation of decreased binding of PARP1 to the METTL3 promoter in HeLa cells after 4-Gy irradiation, determined by ChIP-qPCR assay. (C) HEK293T cells were transfected with the indicated combination of expression constructs for 24 h and incubated with purified proteins, followed by pull-down and immunoblotting with biotin beads. (D–G) Inhibition of METTL3 mRNA (D and F) and protein (E and G) expression by the PARPis NMS-P118 and olaparib (D and E) or knockdown of PARP1 (F and G). (H–K) Observation of the combined effect of radiation and PARPis (H and I) or knocking down PARP1 and rescuing PARP1 (J and K) on the expression of METTL3 mRNA (H and J) and protein (I and K). All data represent the mean ± SD from three independent experiments. Compared with the control, *$p < 0.05$, **$p < 0.01$.

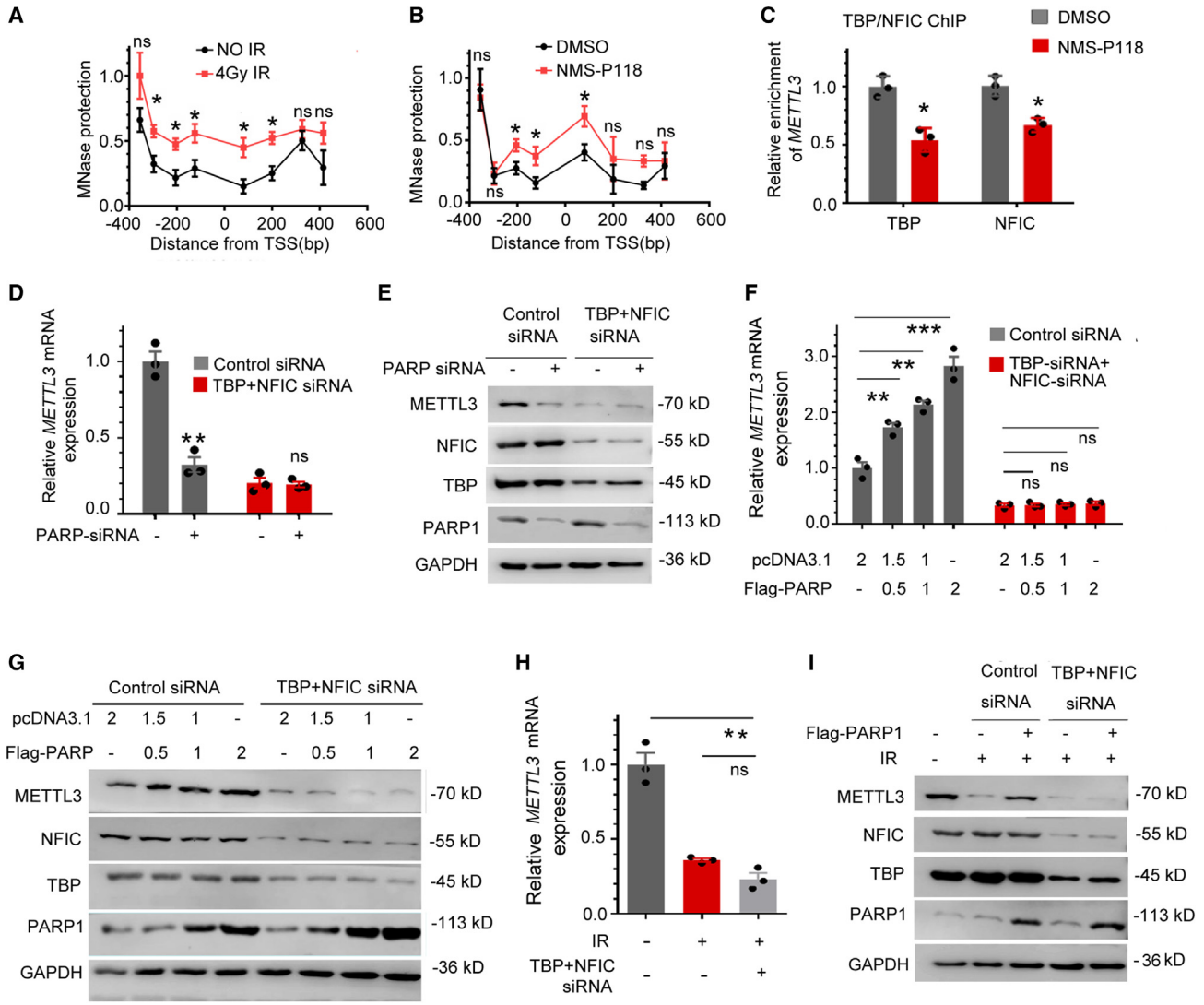

Figure 3. Radiation and PARP1 inhibition suppress the accessibility of METTL3 promoter chromatin

(A and B) The effects of radiation and PARP1 on the openness of METTL3 promoter chromatin, as detected by MNase digestion-qPCR assay. Cells were treated with 4-Gy γ-rays (A) or the PARPi NMS-P118. The chromatin DNA was digested with MNase and then subjected to qPCR assay of METTL3 promoter sequences. (C) The effect of the PARPi NMS-P118 on access of the transcription factors TBP and NFIC to METTL3 promoter chromatin, as detected by a TF-driven ChIP-qPCR assay. (D and E) The effects of depressing TBP and NFIC, and PARP1 on expression of METTL3 mRNA (D) and protein (E). (F and G) TBP/NFIC inhibition attenuated the increase in METTL3 mRNA (F) and protein (G) expression induced by PARP1 overexpression. (H and I) TBP/NFIC inhibition abrogated the rescue effect of overexpressed PARP1 on radiation-depressed METTL3 RNA (H) and protein (I) expression. All data represent the mean ± SD from three independent experiments. *$p < 0.05$, **$p < 0.01$.

including 0.5 h and 2 h after 4 Gy irradiation, respectively. Gene Ontology (GO) and Kyoto Encyclopedia of Genes and Genomes (KEGG) pathway assays were performed to analyze the different peaks of m^{6}A after irradiation. GO analysis showed that IR-induced m^{6}A-modified genes were involved in a variety of biological processes, including regulation of transcription, signal transduction, phosphorylation, apoptotic process (biological process), nucleus, cytoplasm (cellular component), and protein binding (molecular function) (Figure S4A). KEGG enrichment analysis showed that IR-induced m^{6}A-modified genes were enriched in tumor development-related pathways, such as the mitogen-activated protein kinase (MAPK) signaling pathway and p53 pathway (Figure S4B). The m^{6}A motif GGAC was significantly enriched in differential m^{6}A peaks in irradiated cells (Figure 4I) and was especially abundant in the vicinity of the 3′ UTR (Figure S4C).

A total of 2,354 upregulated m^{6}A peaks and 2,579 downregulated m^{6}A peaks were observed in HeLa cells 2 h after 4-Gy irradiation. The coexpression analysis of the differentially expressed mRNAs and m^{6}A methylation is presented as a scatterplot in Figure 4D. According to

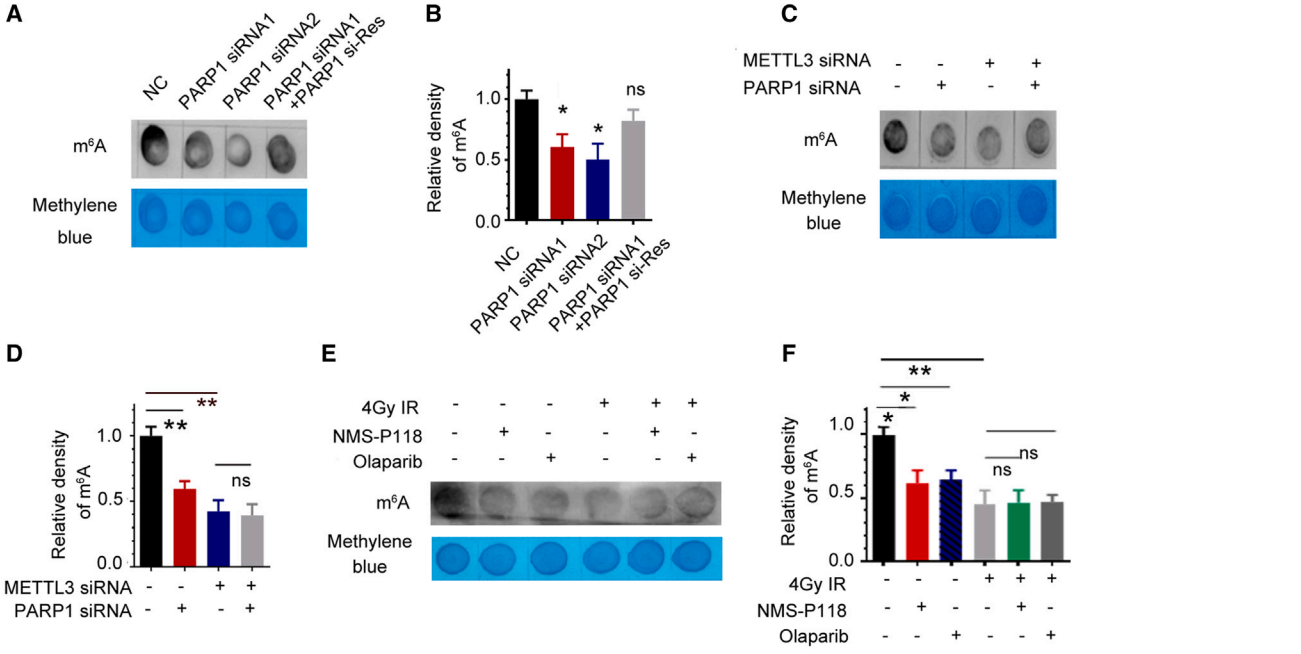

I

Rank	Motif	P-value	log P-pvalue	% of Targets	% of Background	STD(Bg STD)
1		1e-465	-1.073e+03	25.41%	19.69%	49.3bp (55.9bp)
2		1e-294	-6.786e+02	0.44%	0.04%	50.5bp (48.7bp)
3		1e-267	-6.160e+02	0.71%	0.15%	49.1bp (56.1bp)
4		1e-251	-5.802e+02	46.23%	41.17%	50.3bp (55.7bp)
5		1e-226	-5.215e+02	0.59%	0.12%	51.3bp (59.6bp)
6		1e-220	-5.066e+02	44.57%	39.87%	51.3bp (54.5bp)
7		1e-216	-4.993e+02	26.32%	22.30%	50.5bp (56.3bp)
8		1e-215	-4.952e+02	0.52%	0.10%	49.0bp (55.2bp)
9		1e-212	-4.888e+02	11.67%	8.88%	50.1bp (59.8bp)
10		1e-202	-4.670e+02	0.63%	0.15%	49.8bp (49.0bp)

J

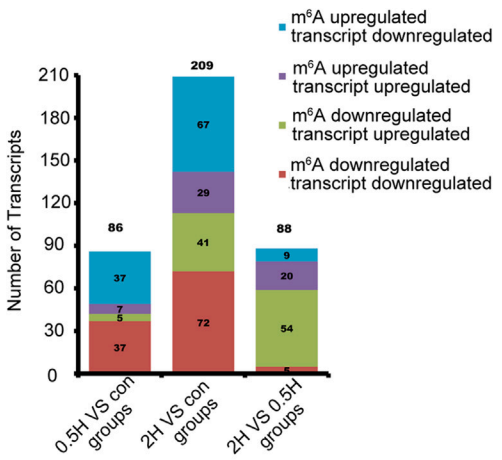

(legend on next page)

the alterations in mRNA expression and m^{6}A methylation, we categorized these differentially expressed genes (greater than 1-fold changes) into four groups (Figure 4J). Specifically, group one included 74 genes (35.4%) that were downregulated in mRNA expression and m^{6}A methylation. Group two included 41 genes (19.6%) with upregulated RNA expression and decreased m^{6}A methylation. Group three included 67 genes (32.1%) with downregulated mRNA expression and upregulated m^{6}A methylation. Group four included 29 genes (13.9%) with upregulated mRNA expression and m^{6}A methylation (Figure 4J).

The top 10 downregulated and upregulated genes with altered m^{6}A modification in the 3′ or 5′ UTR or exon are shown in Figures S4E and S4F. Among all m^{6}A targets identified through m^{6}A-seq, lysophosphatidic acid receptor 5 (LPAR5) is one of the most robust, with significantly decreased levels of m^{6}A modification at its 3′ UTR and transcription after irradiation (Figure S4E). We therefore further focused on LPAR5 m^{6}A modification and its significance in the cellular response to IR.

LPAR5 mRNA is a target of METTL3 catalytic m^{6}A methylation

To confirm whether LPAR5 is a responsive target of the m^{6}A catalytic enzyme METTL3, LPAR5 mRNA and protein expression were first detected in HeLa cells with stable METTL3 siRNA or METTL3 overexpression. Expression of LPAR5 mRNA (Figure S5A) and protein (Figures 5A and S11I) was repressed in HeLa cells with METTL3 silencing. Consistent with this, LPAR5 mRNA (Figure S5B) and protein (Figures 5B and S11J) levels were upregulated in HeLa cells overexpressing METTL3. LPAR5 is a responsive target of METTL3. Expression of METTL3 was repressed in cells after IR, as shown above; thus, expression of LPAR5 was detected in IR-irradiated HeLa cells. We found that LPAR5 mRNA (Figure S5C) and protein (Figures 5C and S11K) expression was depressed in IR-irradiated HeLa cells as well, and IR-induced depression of LPAR5 expression was rescued by overexpression of METTL3. Moreover, the PARPis NMS-P118 and olaparib also depressed expression of LPAR5 mRNA (Figure S5D) and protein (Figures 5D and S11L), which could be rescued by overexpression of METTL3 (Figures 5E and S11M). All of these results indicate that the PARP1-METTL3 axis mediates IR-altered expression of LPAR5.

Given the m^{6}A-seq data showing that the m^{6}A modification of LPAR5 was repressed upon irradiation, we identified whether LPAR5 mRNA was a direct methylation substrate of METTL3. The methylated RNA immunoprecipitation and sequencing (MeRIP)-qPCR results showed that m^{6}A modification of LPAR5 mRNA significantly decreased after irradiation, which could be reversed by overexpressing the exogenous *METTL3* gene (Figure 5F). Furthermore, the m^{6}A modification of LPAR5 mRNA was significantly repressed in HeLa cells after silencing PARP1 (Figure 5G) and METTL3 (Figure 5H). In contrast, the m^{6}A modification of LPAR5 mRNA was significantly enhanced in HeLa cells after overexpressing PARP1 (Figure 5I). All of these data indicate that LPAR5 mRNA is a direct methylation substrate of METTL3.

m^{6}A modification at A1881 mediated by METTL3 stabilizes LPAR5 mRNA

To identify the effect of m^{6}A modification on LPAR5 expression, 3-deazaadenosine (DAA) was used to block RNA methylation, and mRNA expression of LPAR5 was detected by PCR. The abundance of LPAR5 mRNA was repressed after treatment with the methylation inhibitor DAA in the cells (Figure S5E). Given that METTL3-mediated mRNA m^{6}A modification plays an essential role in regulation of mRNA stability,[49,50] to explore how METTL3-mediated m^{6}A modification affects LPAR5 mRNA metabolism, the half-life of LPAR5 mRNA was measured. LPAR5 mRNA degraded faster when METTL3 was stably silenced by siRNA in HeLa (Figure 5J) and A549 (Figure S5F) cells. These results indicate that m^{6}A modification stabilizes LPAR5 mRNA.

Ten potential m^{6}A sites were identified in the LPAR5 3′ UTR. To identify which site(s) were modified by METTL3-mediated m^{6}A on the LPAR5 3′ UTR, luciferase reporters with a series of LPAR5 3′ UTR sequences of wild-type or mutated sites were generated. Reporter assays indicated that all mutated sites except A1881C in the LPAR5 3′ UTR were repressed after METTL3 silencing (Figures 5K and S5G). A1881C locus mutation led to a decrease in m^{6}A methylation (Figure 5L). The LPAR5 3′ UTR sequences containing wild-type or A1881C mutated nucleotides are shown in Figure S5H.

These results indicate that A1881 of the LPAR5 3′UTR is a modified site of m^{6}A. MeRIP-PCR assays further indicated that no additional additive repression was detected at A1881C after METTL3 silencing (Figure 5L), which is consistent with the results of the reporter assay. All of these results indicate that A1881 of LPAR5 is the METTL3-mediated m^{6}A modification site. To confirm the role of m^{6}A modification in LPAR5 mRNA stability, the half-life of A1881C mutant LPAR5 mRNA was measured. Consistent with this, the half-life of A1881C LPAR5 mRNA was dramatically shorter than that of

Figure 4. Depression of PARP1 attenuates m^{6}A methylation of total poly(A)$^+$ RNA and identification of potential m^{6}A targets related to radiation-induced DNA damage

(A and B) PARP1 depression resulted in reduced m^{6}A modification of poly(A)$^+$ RNA in HeLa cells as detected by m^{6}A dot blot assay and quantification. (C and D) The effect of knockdown of PARP1 and METTL3 on m^{6}A modification levels was detected by m^{6}A dot blot assay and quantification. (E and F) The combined effects of radiation and PARPi on m^{6}A modification levels as detected by m^{6}A dot blot assay and quantification. (G and H) siRNA-depressed METTL3 abrogated the increased m^{6}A modification induced by overexpressed PARP1 as detected by m^{6}A dot blot assay and quantification. All data represent the mean ± SD from three independent experiments. *$p < 0.05$, **$p < 0.01$. (I) Sequence logo representing the consensus m^{6}A motifs relative to differential m^{6}A-modified loci identified in 4-Gy γ-ray-irradiated HeLa cells compared with unirradiated cells. Coexpression analysis was performed on transcriptome-wide m^{6}A-seq profiling and RNA-seq profiling. (J) Histogram showing the altering trends of RNA expression and m^{6}A modification pattern of genes in HeLa cells 2 h after irradiation compared with unirradiated cells.

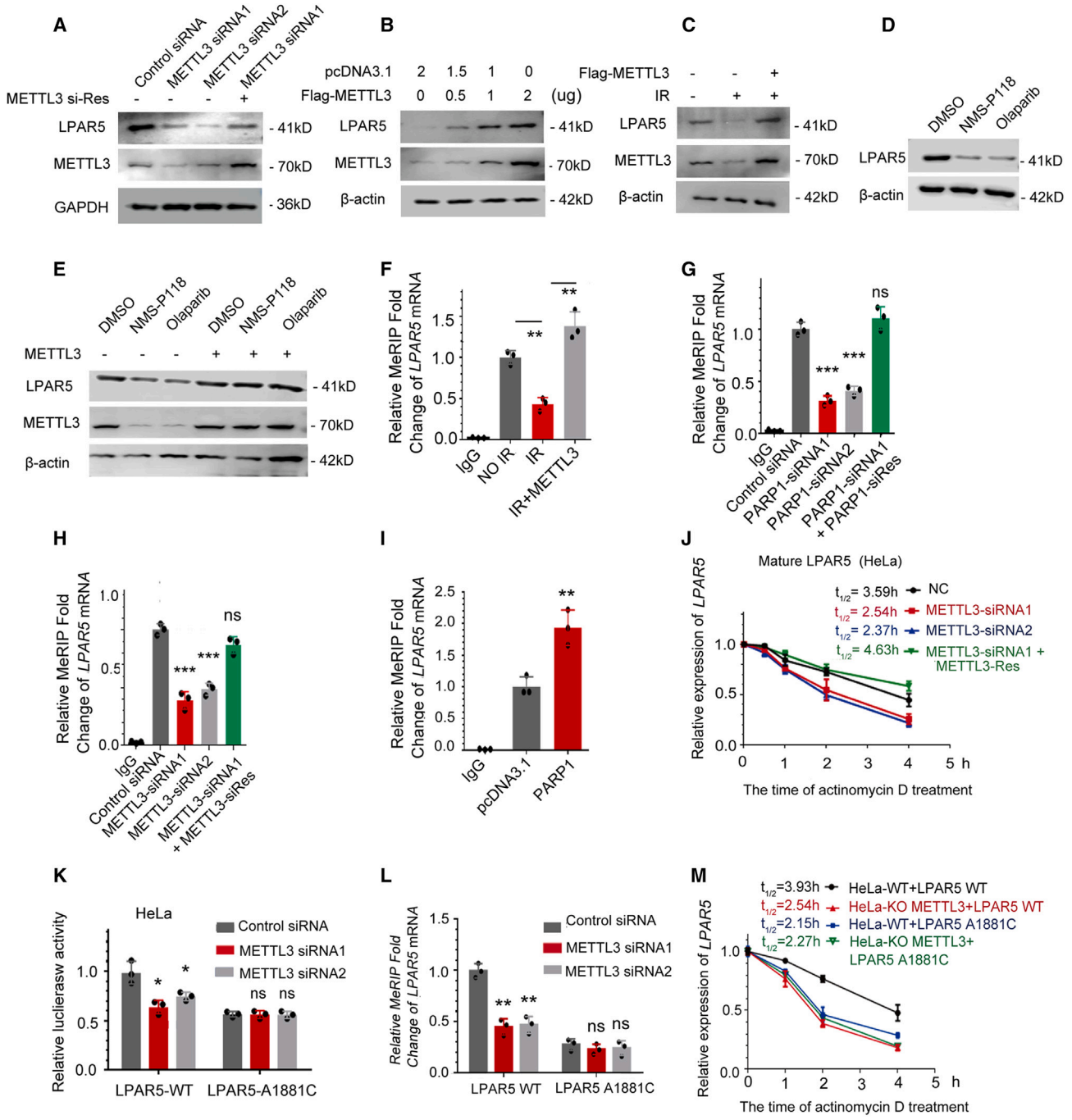

Figure 5. Radiation and PARP1 inhibition depressed LPAR5 expression by modulating METTL3-mediated m^{6}A modification and promoting decay of LPAR5 mRNA

(A) Knockdown of METTL3 reduced the expression of LPAR5 protein. (B) Overexpressing METTL3 increased the expression of LPAR5 protein. (C) Radiation exposure led to depression of LPAR5 protein expression, which was rescued by overexpressing METTL3. (D and E) PARPis depressed the expression of LPAR5 protein (D), which was rescued by overexpressing METTL3 (E). (F) LPAR5 m^{6}A methylation was reduced upon irradiation (F), which could be rescued by overexpressing METTL3. (G and H) LPAR5 m^{6}A methylation was reduced upon knockdown of PARP1 (G) or METTL3 (H). (I) Overexpressing PARP1 enhanced LPAR5 m^{6}A methylation. (J) The half-life of LPAR5 mRNA was shortened by knocking down METTL3 in HeLa cells. (K and L) In HeLa cells, METTL3 knockdown reduced the activity (K) and m^{6}A methylation (L) of LAPR5 3′ UTR WT, and the A1881C mutation led to reduced activity but was no longer affected by METTL3 knockdown. (M) The half-life of LPAR5 WT or A1881C mutant was detected with or without METTL3 knockdown. All data represent the mean ± SD from three independent experiments. *p < 0.05, **p < 0.01.

wild-type (WT) LPAR5 mRNA (Figure 5M). Likewise, knockdown of METTL3 had no additive effect on the half-life of A1881C mutant LPAR mRNA (Figure 5M). Altogether, this shows that A1881 is the METTL3-mediated m^{6}A modification site of LPAR5.

Targeting PARP1-METTL3 axis-mediated LPAR5 m^{6}A methylation signaling pathway patentiates IR-depressed cell proliferation

To investigate the biological role of METTL3 and associated m^{6}A methylation in the cellular response to IR, cell proliferation and viability were detected in HeLa and A549 cells under different types of stress. We found that IR-induced proliferation depression (Figures 6A and 6B) and apoptosis (Figures 6C, S6A, and S6B) were attenuated in cells overexpressing METTL3. We further identified that apoptosis induced by suppressing PARP1 (Figure 6D), the PARPi, or combined treatment with IR and PARPi was also rescued by overexpression of METTL3 in HeLa and A549 cells (Figures 6E, S6C, and S6E).

Because LPAR5 mRNA was identified as a methylation target of METTL3 in response to γ-ray irradiation in our m^{6}A-seq assay described above, and LPAR5 expression was repressed after IR or by METTL3 silencing, we identified whether METTL3-controlled IR-induced apoptosis is associated with inhibition of LPAR5. Interestingly, apoptosis was induced in cells by silencing LPAR5 (Figures 6F and S7A). Apoptosis induced by silencing METTL3 can be rescued by overexpressing LPAR5, and the rescue effects of WT LPAR5 were more significant than those of the LPAR5 A1881C mutant, which expresses a relatively unstable mRNA transcript because of loss of the m^{6}A-modified locus, in HeLa and A549 cells (Figures 6G and S7B). We then identified the role of LPAR5 in radiation-induced cell apoptosis. The results demonstrated that IR-induced apoptosis was largely attenuated by overexpressing LPAR5 in HeLa and A549 cells; consistent with this, the effect of LPAR5 WT was stronger than that of the A1881C mutant (Figures 6H and S7C).

To further identify whether the activity of METTL3 in IR-induced cell apoptosis is associated with LPAR5, we overexpressed METTL3 in the presence or absence of LPAR5 siRNA in HeLa and A549 cells. We found that overexpressing METTL3 attenuated the IR-induced apoptosis, and this attenuation could be counteracted by silencing LPAR5 (Figures 6I, 6K, and S7D) or PARP1 (Figures 6J and S8A). The PARPi further promoted apoptosis induced by IR, which could be eliminated by overexpressing METTL3 or LPAR5 (Figures 6K and S8B). All of these results indicate that the PARP1-METTL3-LPAR5 m^{6}A axis plays an important role in IR-induced apoptosis.

Targeted inhibition of METTL3 suppresses tumor growth and synergizes with radiation therapy *in vivo*

Inhibition of METTL3 augmented IR-induced apoptosis, which is mediated by the LPAR5 m^{6}A modification pathway. To reveal the clinical relevance and significance of the PARP1-METTL3-LPAR5 regulatory axis, immunohistochemistry staining was performed in a tissue array of cervical cancer and paired para-tumor cervical tissue. The results showed that the expression levels of PARP1, METTL3, and LPAR5 were significantly increased in cervical carcinomas compared with the paired para-tumor cervical tissues (Figures 7A–7D and S10), and the expression level of LPAR5 was significantly correlated with METTL3 (Figure 7E).

STM2457 is a newly developed METTL3 inhibitor for treatment of myeloid leukemia.[51] To test the antitumor effect of targeting METTL3 as a combination strategy with radiotherapy on solid cancers, we initially developed a HeLa cell line with METTL3 knockout (KO) (Figure S9A) to identify whether METTL3 KO affects xenograft tumor growth. The results indicated that the volume and weight of tumor grafts originating from METTL3-KO cells were much smaller than those of WT cell tumors (Figures S9B and S9E). To investigate the antitumor effect of the METTL3-targeted inhibitor STM2457, HeLa cells were injected subcutaneously into mice and then randomly divided into 4 groups: STM2457 treatment alone, irradiated alone, irradiation combined with STM2457 treatment, and control. The mice were given STM2457 or vesicle control treatment half an hour before irradiation. Tumor volumes were measured every 3 days, starting 1 day after treatment (Figure 7F). The mice were sacrificed 21 days after treatment, and the tumors were measured and weighed (Figures 7G, 7H, and S9F). The results showed that tumor growth and the volume and weight of tumors in the STM2457 treatment group and irradiation group were markedly reduced in comparison with those in the vehicle control group (Figures 7F–7H). STM2457 treatment synergized with radiotherapy to inhibit tumor growth. All of these results indicate that METTL3-targeted inhibition is a promising combination therapy strategy for radiotherapy.

DISCUSSION

METTL3 is a key enzyme that catalyzes m^{6}A modification. To date, the upstream regulators and the mechanism controlling METTL3 expression, especially under environmental stress or therapeutic scenarios of diseases, have not been well delineated. Here, we report that PARP1 controls the chromatin openness of the METTL3 promoter. Radiation exposure and PARPi treatment lead to dissociation of PARP1 from the METTL3 promoter chromatin, which attenuates the accessibility of the transcription factors NFIC and TBP to the METTL3 promoter and consequently inactivates METTL3 transcription and its mediated m^{6}A modification of poly(A)$^+$ RNA, including LPAR5 mRNA, which is an emerging prognostic indicator of various cancers.[52–56] Radiation exposure and PARP1 inactivation reduced METTL3 expression, consequently decreasing m^{6}A modification of LPAR5, which led to proliferation inhibition and apoptosis of cells. PARP1 is necessary for activating transcription of *METTL3* by promoting the accessibility of METTL3 promoter chromatin, which is important for recruitment and binding of the positive transcription factors NFIC and TBP. We demonstrated for the first time that a PARPi suppresses METTL3 expression and reduces its m^{6}A modification. In addition, we also identified LPAR5 as a target of METTL3 and showed that abrogation of LPAR5 mRNA m^{6}A modification at the A1881 locus decreased its stability.

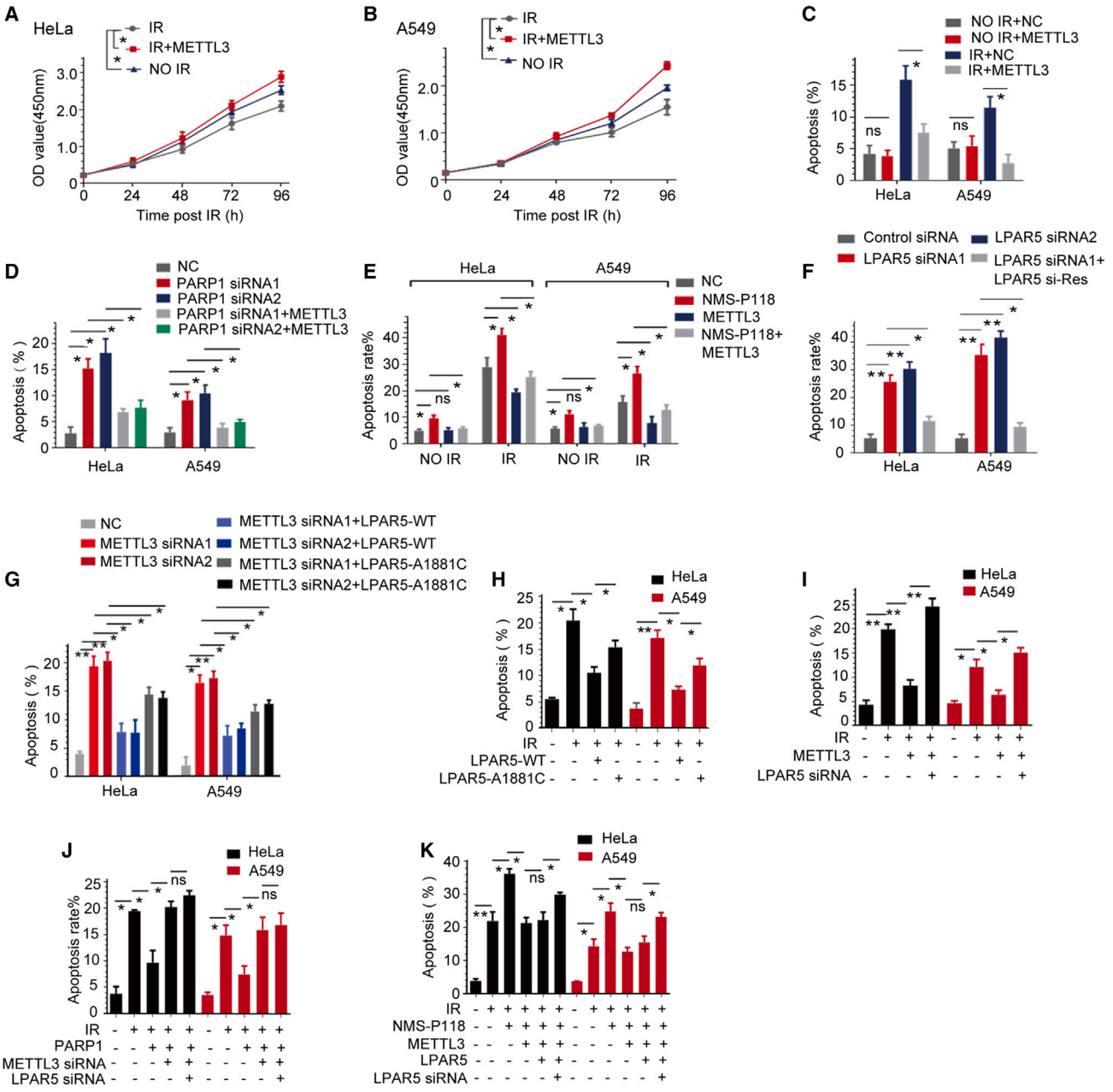

Figure 6. Irradiation promotes apoptosis and inhibits cancer cell proliferation through the PARP1-METTL3-m^{6}A-LPAR5 axis

(A–C) overexpressing METTL3 attenuated radiation-induced proliferation inhibition (A and B) and apoptosis induction (C) in HeLa and A549 cells. (D and E) Apoptosis induced by PARP1 depression (D), PARPi, or irradiation or combined treatment of IR and PARPi (E) was partially rescued by overexpressing METTL3. (F) LPAR5 knockdown induced apoptosis in HeLa and A549 cells. (G and H) Increased occurrence of apoptosis by knocking down METTL3 (G) or irradiation (H) was attenuated by overexpressing LPAR5-WT or LPAR5-A1881C but to a lesser extent by LPAR5-A1881C. (I) Apoptosis induced by radiation was attenuated by overexpressing METTL3 but not by overexpressing METTL3 and simultaneously knocking down LPAR5. (J and K) Verification of radiation-induced apoptosis via the PARP1-METTL3-LPAR5 axis. (J) Effects of LPAR5 knockdown, PARP1 overexpression, or METTL3 knockdown on apoptosis in irradiated HeLa cells and A549 cells. (K) Effects of overexpressing LPAR5, METTL3, NMS-P118 treatment or combination treatment on apoptosis induction in irradiated HeLa cells and A549 cells. All data represent the mean ± SD from three independent experiments. *$p < 0.05$, **$p < 0.01$.

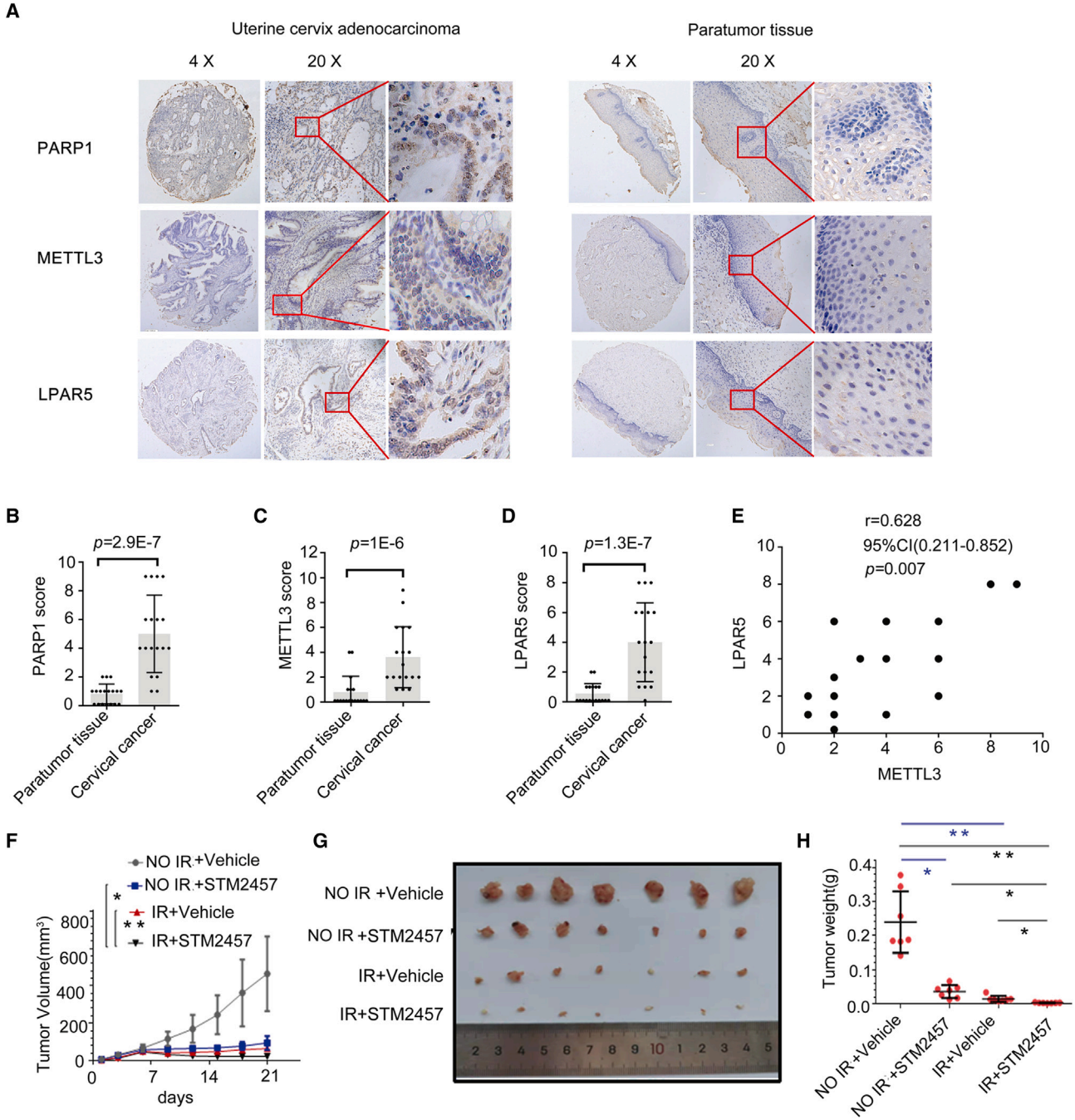

Figure 7. Targeted inhibition of METTL3 suppresses tumor growth and exhibits a synergistic effect with radiation *in vivo*

(A) Representative images of immunohistochemistry (IHC) analysis of PARP1, METTL3, and LPAR5 in a tumor tissue array of uterine cervix adenocarcinoma. The tissue array was composed of human cervical cancers and paired para-tumor tissues. (B–D) Quantitative comparisons between cervical cancers and paired para-tumor tissues for PARP1, METTL3, and LPAR5 expression IHC analyses. (E) Correlation analysis of METTL3 and LPAR5 expression in cervical cancers. (F–H) Tumor suppression by a small-molecule inhibitor of METTL3 and synergistic effect with radiation. (F) The tumor sizes in each group were monitored every 3 days starting from 1 day after radiation treatment. (G and H) Tumor sizes and weights in each group 21 days after radiation treatment. n = 7, *p < 0.05, **p < 0.01.

It has been reported that DNA damage can recruit METTL3 to the damage site, resulting in m^{6}A modification of DNA damage-related RNA for homologous recombination (HR).[57] In this study, we found that the transcriptional activity of METTL3 was reduced upon irradiation, which led to inhibition of m^{6}A modification and promoted cell apoptosis. Our study demonstrates the role of METTL3 in radiation-induced DNA damage in another aspect. Similar to our findings, some studies have noted that METTL3 can enhance the repair efficiency of γ-ray damage in glioma cells and pancreatic cancer cells by regulating the RNA stability of downstream target molecules.[39,41] Here, we demonstrated that METTL3 modulates cellular radiosensitivity by regulating the m^{6}A modification of LPAR5, mediating radiation-induced apoptosis and increasing cancer cell-killing effects.

PARP1 is a constitutive DNA repair factor acting as a DNA break sensor and DDR protein modulator.[58,59] PARP1 is also a nucleosome-binding nucleoprotein involved in a variety of nuclear processes, including modulation of chromatin structure/accessibility and transcription.[45,48,60] Given that PARP1 is rapidly recruited and activated by DNA double-strand breaks (DSBs), it is surprising that PARP1-mediated METTL3 transcription is inhibited upon irradiation. The phenomenon of radiation-attenuated m^{6}A modification of total mRNA in a dose-dependent manner indicates that, upon IR-induced DNA damage, the dynamics of PARP1 binding to METTL3 promoter region chromatin could be altered, which affected the transcriptional activity of the target gene. PARP1 consists of multiple functional domains, including the N-terminal DBD containing three zinc fingers, the middle automodification/BRCT domain, the C-terminal protein-interacting WGR domain, and the catalytic domain. PARPis can suppress PARP1 binding to chromatin. The enzymatic activity of PARP1 can be activated either by the DNA damage signal or by interacting with histone H4 in a phosphorylated H2Av histone-bearing nucleosome.[48] The interaction between the N-terminal DBD and damaged DNA leads to short-term binding and activation of PARP1 to initiate the DNA repair pathway at a specific point.[48] Automodified PARP1 loses its ability to interact with DNA and is released from chromatin.[47,48,60,61] PARP1 binding to nucleosomes with its C-terminal domain leads to long-term activation of PARP1 chromatin by interacting with histone H4, which results in continuous production of PAR (pADPr) to maintain chromatin in a loosened state and accessibility to transcription factors.[48] Because pADPr has a short life, it can be degraded by pADPr glycohydrolase (PARG) at any time. Thus, to maintain a chromatin-loosening and gene transcription active state, sustained chromatin binding and activation of PARP1 are needed. Based on our results and the accumulated information regarding the biochemical and biological characteristics of PARP1 binding chromatin, we propose a mechanistic explanation for PARP1 modulating chromatin accessibility and METTL3 promoter activity in response to radiation-induced DNA damage. Under normal growing conditions, PARP1 is recruited and binds to the chromatin around the METTL3 promoter region and is sustainably activated in an H4-dependent manner to produce pADPr, which maintains chromatin openness and active transcription. Upon IR-induced DNA damage, PARP1 is auto-PARylated and prompts access of DDR and repair proteins (DDRPs) to DNA damage to facilitate DNA repair. On the other hand, automodified PARP1 loses its ability to bind DNA and may be released from chromatin, resulting in chromatin remodeling and temporary silencing of gene transcription until *de novo* recruitment of PARP1.

Biochemical studies have shown that PARP1 can facilitate nucleosome disassembly and result in chromatin relaxation.[62,63] It has also been reported that knockdown of PARP1 decreased binding of the transcription factor TBP at the promoters of positively regulated genes,[64] which coincides with our findings. Our data demonstrate that PARP1 modulates the accessibility of METTL3 promoter chromatin and its transcriptional activity. Upon radiation-induced DNA damage or PARP1 inhibition, access of TBP and NFIC to METTL3 promoter chromatin and its transcriptional activity is suppressed, which results in downregulation of associated m^{6}A modification and affects the function of a series of target mRNAs, including LPAR5. Decreased m^{6}A modification of LPAR5 mRNA at the motif around the A1881 site leads to its unstable and decreased expression after irradiation. LPAR5 is a recently discovered member of the LPAR family; it is frequently dysregulated in a variety of tumors and mediates tumor growth, invasion, and metastasis.[54,56,65–67] Alteration of m^{6}A modification and mRNA stability of LPAR5 in response to IR implies that LPAR5 could play an important role in tumor suppression of radiotherapy.

PARP1, a founding member of the ADP-ribosyl transferase family, has been the most widely investigated member of this family of enzymes. Inhibitors targeted by PARP1 have been constantly developed for targeted therapy of tumors, especially with mutations in the essential HR genes BRCA1 and BRCA2, which is called synthetic lethality.[4,68] In this study, we revealed that PARP1 regulates METTL3 and mediates m^{6}A modification by modulating chromatin accessibility in the cellular response to radiation-induced DNA damage. There is no doubt that there are functional targets worth discovering and investigating in this pathway. The mechanism of PARP1 dissociation from the chromatin around the METTL3 promoter region after IR still needs further investigation. Further clarification is needed of how PARP1 affects the mechanism by which NFIC and TBP bind to the METTL3 promoter region. The mechanism may be mediated by PARylation of histones or by PARylation of TBP and NFIC. We found that DNA damage not only regulates gene expression at the transcriptional level but also performs the same function at the translational level. However, the biological significance of IR in regulating m^{6}A modification and mRNA translation through METTL3 remains to be further studied. We verified LPAR5 as a direct downstream target of this PARP1/MRETTL3-m^{6}A modification pathway. After irradiation, METTL3-mediated m^{6}A modification and expression of LPAR5 mRNA were significantly decreased, which contributed to apoptosis induction. LPAR5 regulates a variety of malignant properties of cancer cells, as mentioned above. Increased expression of LPAR5 is considered a major cause that led to chemoresistance, and knocking down LPAR5 enhances cancer cells to cisplatin (CDDP).[53,69] Here, we revealed that PARPi

and radiation inhibit METTL3-mediated m^{6}A modification, which prompts apoptosis induction at least partially by targeting LPAR5 signaling. A molecular inhibitor of METTL3 was further confirmed to markedly suppress tumor growth and exhibited an additive inhibitory effect with radiation *in vivo*.

Conclusions

In conclusion, PARP1 modulates the openness of METTL3 promoter chromatin to regulate RNA m^{6}A modification. Upon radiation-induced DNA damage or PARPi treatment, PARP1 disassociates from *METTL3* promoter chromatin, which results in attenuated accessibility of the METTL3 promoter, consequently decreasing METTL3 expression and the associated m^{6}A modification of poly(A)$^+$ RNA. The A1881 site at the 3′ UTR of LPAR5 mRNA is one of the targets of the PARP1-METTL3-m^{6}A modification axis, which plays an important role in determination of cell radiosensitivity. This new aspect of PARP1 function in regulating the RNA m^{6}A modification paradigm provides favorable evidence and knowledge for developing and precisely applying PARP inhibitors for cancer therapy as well as improving the effectiveness of radiotherapy in cancer treatment.

MATERIALS AND METHODS

Cell culture

HeLa cells and A549 cells were purchased from the American Type Culture Collection (ATCC). HeLa cells and A549 cells were grown in DMEM (HyClone) containing 10% fetal bovine serum (FBS; HyClone and PAN) and 1% penicillin-streptomycin.

Inhibitors, plasmids, and siRNAs

Inhibition of PARP1 was performed by treating cells with 10 μM PARPi (NMS-P118 and olaparib) for 6 h.

The conding sequences (CDS) of METTL3 was cloned into pEGFP-C1, and the full sequence of LPAR5 was cloned into pcDNA3.1. The CDS of PARP1 was cloned into pcDNA3.1 to generate an overexpression plasmid. The promoter of METTL3 was cloned into pGL3-basic, and the 3′ UTR of LPAR5 was cloned into pmirGLO to generate a fusion reporter gene plasmid.

cDNAs encoding the PARP1 protein or their truncated variants were cloned into pcDNA3.1 following the standard molecular cloning technique.

For PARP1, LPAR5, NFIC, TBP, and METTL3 knockdown, two synthesized duplex RNAi oligos targeting human mRNA sequences from Sigma were used. A scrambled duplex RNA oligo (5′-UUCUCC GAACGUGUCACGU-3′) was used as an RNA control. Transfection was performed using Lipofectamine 2000 reagent (Invitrogen) with vector control, plasmid construct, siRNA negative control (siNC), or siRNAs according to the manufacturer's instructions. The working concentration of siRNA was 50 nM, and the incubation time was 24 h. The siRNA sequences are listed in Table S1.

In vivo subcutaneous implantation and radiation models

For the subcutaneous implantation model, stable METTL3 KO HeLa cells were constructed via CRISPR-Cas9 technology (CYAGEN, CRISPR gRNA). METTL3 KO or WT HeLa cells were injected subcutaneously into BALB/c nude mice. For radiation models, 1×10^7 WT HeLa cells were injected into the backs of nude mice. For the experimental therapy test of the METTL3 inhibitor STM2457, after the transplanted tumor reached approximately 5 mm in diameter, the mice were randomly divided into 4 groups: the control group, irradiation group, STM2457 group, and irradiation combined with STM2457 group (the dose of STM2457 was 50 mg/kg, and the radiation dose was 4 Gy). Tumor growth (size) was measured, and data were recorded after inoculation. After 2 weeks, the mice were killed, and the tumors were resected and weighed. The animal experiments were approved (IACUC-DWZX-2021-711) by the Animal Care and Use Committee at the Military Academy of Medical Sciences and complied with the Laboratory Animal Guidelines of Welfare and Ethics of China.

Poly(A)$^+$ RNA m^{6}A quantification

The poly(A)$^+$ RNA was isolated using a Dynabeads mRNA Direct Purification Kit (Thermo Fisher Scientific, 18068015) according to the manufacturer's instructions. mRNA quality was analyzed by NanoDrop. An m^{6}A RNA methylation quantification kit (Abcam, ab185912) was used to measure the m^{6}A content in the mRNA. Briefly, 200 ng mRNA was coated on assay wells. Capture antibody solution and detection antibody solution were then added to assay wells separately at a suitable diluted concentration, following the manufacturer's instructions. The m^{6}A levels were quantified colorimetrically by reading the absorbance of each well at a wavelength of 450 nm, and then calculations were performed based on the standard curve.

RNA extraction and quantitative real-time PCR analysis

Total RNA was isolated using TRIzol. One microgram of RNA was reverse-transcribed into cDNA with ReverTra Ace qPCR RT Master Mix with gDNA Remover (TOYOBO, FSQ-301) according to the manufacturer's instructions. Quantitative real-time PCR analysis was performed with 1 μL cDNA using THUNDERBIRD SYBR qPCR Mix (TOYOBO, QPS-201). Actin was used as an endogenous control. Each sample was run in triplicate. The quantitative PCR primers are listed in Table S1.

m^{6}A dot blot assay

Poly(A)$^+$ RNA was isolated using a Dynabeads mRNA Direct Purification Kit (Thermo Fisher Scientific, 18068015) according to the manufacturer's instructions. mRNA quality was analyzed by NanoDrop. Poly(A)$^+$ RNAs (300 ng) were spotted onto a nylon membrane (Beyotime) and UV crosslinked to the membrane (1,200 μJ, 25–50 s). The nylon membrane was stained with 0.02% methylene blue for 5 min and then washed with ribonuclease-free water for 15 min until the background color became thinner. Then, the membrane was blocked with 5% nonfat dry milk (in 1× PBST) for 1 h and incubated with a specific anti-m^{6}A antibody (1:1,000 dilution,

Synaptic Systems, 202003) overnight at 4°C. Then, horseradish peroxidase (HRP)-conjugated goat anti-rabbit immunoglobulin G (IgG) was added to the membrane for 1 h at room temperature, and the blot was visualized using SuperSignal West Pico Plus Chemiluminescent Substrate (Thermo Fisher Scientific, TL275133).

m^{6}A MeRIP-qPCR

Poly(A)$^+$ RNA was isolated using a Dynabeads mRNA Direct Purification Kit (Thermo Fisher Scientific, 18068015) according to the manufacturer's instructions. Chemically fragmented mRNA (10 μg) was incubated with m^{6}A antibody for immunoprecipitation according to the standard protocol of the RiboMeRIP m^{6}A Transcriptome Profiling Kit (RIBO, C11051-1). Enrichment of m^{6}A-containing mRNA was then analyzed through qRT-PCR or high-throughput sequencing. Library preparation and high-throughput sequencing were performed by Novogene (OmicStudio, Beijing, China). The qPCR primers are listed in Table S1.

mRNA stability assay

To assess RNA stability, the cells were incubated with actinomycin D (Santa Cruz Biotechnology) at 5 mg/mL for the indicated times. The cells were collected, and RNA samples were extracted for qPCR analysis.

Dual-luciferase reporter assay

A luciferase reporter assay was performed with the Dual-Luciferase Reporter Assay System (Promega, E1910) according to the manufacturer's instructions. Cells were seeded into 24-well plates 1 day before transfection.

To evaluate the effect of irradiation on the transcriptional activity of the METTL3 promoter, after 24 h, the cells were cotransfected with the pRL-CMV vector and pGL3-METTL3 containing the −2000/+1 sequence of the METTL3 promoter.

To evaluate the potential roles of the 3′ UTR in LPAR5 expression, the WT or mut-(1–10) of the 3′ UTR of LPAR5 was inserted behind the F-Luc coding region. pmirGLO-LPAR5-3′ UTR-WT and pmirGLO-LPAR5-3′ UTR-Mut-(1–10) were transfected into WT or METTL3 knockdown cells for 24 h. *Renilla* luciferase (R-Luc) was used to normalize firefly luciferase (F-Luc) activity. Each group was analyzed at least three times.

Western blot analysis

Cells were lysed with radio-immunoprecipitation assay (RIPA) buffer containing 5 mM EDTA, PMSF, and phosphatase inhibitor cocktail. Cell extracts were centrifuged for 15 min at 12,000 × *g*, and supernatants were collected. Approximately 40 μg of total protein was resolved by SDS-PAGE, transferred onto nitrocellulose (NC) membranes, blocked with 5% nonfat milk at room temperature for 2 h, and incubated with primary antibodies. After being washed three times, the membrane was incubated with HRP-conjugated secondary antibodies (1: 4,000 dilution) for 1 h at room temperature, and the blot was visualized using SuperSignal West Pico Plus Chemiluminescent Substrate (Thermo Fisher Scientific, TL275133).

Proliferation and apoptosis assay

Cells (1.5×10^3) were seeded into 96-well plates and incubated at 37 °C in a humidified 5% CO_2 atmosphere. Cellular proliferation was measured with Cell Counting Kit-8 (DOJINDO, SJ608). Briefly, 10 μL/well CCK8 solution was added at the indicated times, and then the cells were incubated at 37 °C for 3 h. The absorbance at 450 nm was recorded by a microplate reader.

To assess cell apoptosis, after being treated with trypsin, the cells were collected and washed with PBS twice. Four microliters of PI (propidium iodide) and 4 μL of FITC (fluorescein isothiocyanate) (DOJINDO; AD10) were added after the cells were pelleted and resuspended in 400 μL of 1× binding buffer. Apoptosis was detected by flow cytometry after 15 min of incubation in the dark at room temperature.

DNA pull-down assay

The biotinylated promoter of METTL3 was used to determine the interaction between the promoter and transcription factor. After PCR was used to label the promoter of METTL3, it was resolved by agarose gel electrophoresis. The promoter of METTL3 was recycled using a SanPrep Column DNA Gel Extraction Kit (Sang, B518131) according to the manufacturer's instructions. Extraction of nuclear proteins was performed using the Nucleoprotein Extraction Kit (Sangon, C500009) according to the manufacturer's instructions. Approximately 10 μg of METTL3 promoter and 1,000 μg of nucleoprotein were bound to streptavidin-agarose (Millipore, S1638) at 4°C with end-over-end rotation for 1 h. The beads were washed twice with 1 mL PBS, and the proteins bound to the beads were analyzed by 10% SDS-PAGE with Coomassie brilliant blue staining.

ChIP assay

ChIP assays were performed using the EZ ChIP Kit (17-371, Millipore). Briefly, cells were cross-linked with 1% formaldehyde, lysed, and sonicated on ice to generate DNA fragments with an average length of 200–1,000 bps. Precleared DNA of each sample was saved as an input fraction. Precleared DNA was then used for immunoprecipitation with 5 μg of ChIP-grade antibody specifically against PARP1 (13371-1-AP, Proteintech). IgG was included as a nonspecific control. DNA was eluted and purified, followed by qRT-PCR using specific primers.

MNase protection assay

For MNase experiments, 1×10^7 cells were washed twice with cold PBS. The samples were divided into two aliquots, one of which was digested with MNase to yield mononucleosomes, and the other was lightly sonicated (Figure S4J). After centrifugation, cells were permeabilized with 0.03% Triton X-100 and 10% fetal calf serum in PBS and incubated for 10 min at 37 °C. After centrifugation (1,000 × *g* for 5 min), cells were resuspended in reaction buffer (150 mM sucrose, 50 mM Tris-Cl (pH 7.5), 50 mM NaCl and 2 mM $CaCl_2$). The chromatin was digested with MNase (2 U/mL) for 20 min and

quenched with EGTA. For low-coverage nucleosome position maps, MNase-digested DNA was subjected to real-time PCR with primers designed according to the predicted nucleosome positions, amplifying ~100 bp nonoverlapping fragments of DNA regions between −400 and +400 bp of the Cga and Lhb genes. The enrichment of MNase-digested DNA relative to sonicated genomic DNA at specific genomic locations was determined by qPCR. The PCR primers are listed in Table S1.

Immunohistochemistry analysis of the tissue array

A tissue array chip of cervical cancer and matched para-tumor was purchased from Zhongke Guanghua. This study was approved by the Ethics Committee of the Military Academy of Medical Sciences (AF/SC-08/02.217). After deparaffinization and antigen retrieval, the array was incubated with anti-PARP1 antibody (dilution 1:200, Proteintech, 13371-1-AP), anti-METTL3 antibody (dilution 1:200, Proteintech, 15073-1-AP), or anti-LPAR5 antibody (dilution 1:25, Sangon Biotech, D260792) at 4 °C overnight. The array was rinsed in PBS and incubated with HRP-labeled goat anti-rabbit IgG for 30 min at room temperature. Positive expression was visualized using DAB. The outcome signals were scored according to the percentage of positive cells and staining intensity. Staining intensity was assessed on a scale from 0–3 (0 = negative, 1 = weak, 2 = moderate, 3 = strong), and the percentage of positive cells (0, <5%; 1, 6%–25%; 2, 26%–50%; 3, 51%–75%; and 4, 76%–100%) was assessed semiquantitatively. The final scores (0–12) were then calculated by multiplying these 2 values.

In vivo subcutaneous and radiation mouse models

For the subcutaneous implantation model, stable METTL3 KO HeLa cells or WT HeLa cells were injected subcutaneously into BALB/c-Nude mice (1×10^7 cells/0.1 mL/mouse). For radiation models, 1×10^7 WT HeLa cells were injected into the backs of nude mice. They were randomly divided into 4 groups: control group, irradiation group, STM2457 group, and irradiation combined with STM2457 group. After the transplanted tumor reached approximately 5 mm in diameter, the mice were orally administered STM2457 (50 mg/kg body weight, p.o.) and/or control oil (0.1 mL/mouse, p.o.). Approximately half an hour later, the tumor tissue was exposed to 4-Gy irradiation. Tumor growth was observed, and data were recorded after inoculation. After 2 weeks, the mice were killed, and the tumors were resected and weighed. The experimental procedures and animal use were performed with approval of the Institutional Animal Care and Use Committee of the Laboratory Animal Center. Animal experiments were carried out according to the Control of Animal Laboratory of the Academy of Military Medical Sciences and the principles on animal works (IACUC-DWZX-2021-711).

Quantification and statistical analysis

Data are presented as the mean ± SEM or SD. Statistical analyses were performed in GraphPad Prism 6. An unpaired two-tailed Student's t test was used to compare differences between two groups with a significance of $p < 0.05$. One-way analysis of variance with multiple comparisons tests was used to compare three or more groups with a significance of $p < 0.05$.

DATA AND CODE AVAILABILITY

The datasets generated during the current study are available from the corresponding author upon reasonable request.

SUPPLEMENTAL INFORMATION

Supplemental information can be found online at https://doi.org/10.1016/j.ymthe.2023.07.018.

ACKNOWLEDGMENTS

This study was supported by grants from the National Natural Science Foundation of China (82230108, 82103784, and 32171238).

AUTHOR CONTRIBUTIONS

X.Y.S. and S.S.G. performed most of the experiments. D.X., H.L., S.C., Y.H., J.J., H.G., J.L. and D.L. assisted with the experiment and critical reagent preparation. Y.L. and Y.Y. provided technical help with tissue array analysis. D.X. and X.H. performed the bioinformatics analysis. P.K.Z. and C.J.B. contributed to experimental design, guidance, and quality control. R.H. and P.K.Z. conceived the project, analyzed the data, and finalized the figures. X.Y.S. and S.S.G. drafted the initial manuscript, and R.H. and P.K.Z. critically reviewed and revised the final manuscript.

DECLARATION OF INTERESTS

The authors declare no competing interests.

REFERENCES

1. Cole, A.J., Dickson, K.A., Liddle, C., Stirzaker, C., Shah, J.S., Clifton-Bligh, R., and Marsh, D.J. (2021). Ubiquitin chromatin remodelling after DNA damage is associated with the expression of key cancer genes and pathways. Cell. Mol. Life Sci. *78*, 1011–1027.
2. Reyes, A.A., Marcum, R.D., and He, Y. (2021). Structure and Function of Chromatin Remodellers. J. Mol. Biol. *433*, 166929.
3. Curtin, N.J., and Szabo, C. (2020). Poly(ADP-ribose) polymerase inhibition: past, present and future. Nat. Rev. Drug Discov. *19*, 711–736.
4. Huang, R., and Zhou, P.K. (2021). DNA damage repair: historical perspectives, mechanistic pathways and clinical translation for targeted cancer therapy. Signal Transduct. Target. Ther. *6*, 254.
5. Ooi, S.K., Sato, S., Tomomori-Sato, C., Zhang, Y., Wen, Z., Banks, C., Washburn, M.P., Unruh, J.R., Florens, L., Conaway, R.C., et al. (2021). Multiple roles for PARP1 in ALC1-dependent nucleosome remodelling. Proc. Natl. Acad. Sci. USA, 118.
6. Luo, X., and Kraus, W.L. (2012). On PAR with PARP: cellular stress signaling through poly(ADP-ribose) and PARP-1. Genes Dev. *26*, 417–432.
7. Alemasova, E.E., and Lavrik, O.I. (2019). Poly(ADP-ribosyl)ation by PARP1: reaction mechanism and regulatory proteins. Nucleic Acids Res. *47*, 3811–3827.
8. Schuhwerk, H., Atteya, R., Siniuk, K., and Wang, Z.Q. (2017). PARPing for balance in the homeostasis of poly(ADP-ribosyl)ation. Semin. Cell Dev. Biol. *63*, 81–91.
9. Kaufman, B., Shapira-Frommer, R., Schmutzler, R.K., Audeh, M.W., Friedlander, M., Balmaña, J., Mitchell, G., Fried, G., Stemmer, S.M., Hubert, A., et al. (2015). Olaparib monotherapy in patients with advanced cancer and a germline BRCA1/2 mutation. J. Clin. Oncol. *33*, 244–250.
10. Lord, C.J., and Ashworth, A. (2017). PARP inhibitors: Synthetic lethality in the clinic. Science *355*, 1152–1158.
11. Ray Chaudhuri, A., and Nussenzweig, A. (2017). The multifaceted roles of PARP1 in DNA repair and chromatin remodelling. Nat. Rev. Mol. Cell Biol. *18*, 610–621.

12. Buckley, A.M., Lynam-Lennon, N., O'Neill, H., and O'Sullivan, J. (2020). Targeting hallmarks of cancer to enhance radiosensitivity in gastrointestinal cancers. Nat. Rev. Gastroenterol. Hepatol. *17*, 298–313.

13. Huang, R.X., and Zhou, P.K. (2020). DNA damage response signaling pathways and targets for radiotherapy sensitization in cancer. Signal Transduct. Target. Ther. *5*, 60.

14. Arina, A., Gutiontov, S.I., and Weichselbaum, R.R. (2020). Radiotherapy and Immunotherapy for Cancer: From "Systemic" to "Multisite". Clin. Cancer Res. *26*, 2777–2782.

15. Durant, S.T., Zheng, L., Wang, Y., Chen, K., Zhang, L., Zhang, T., Yang, Z., Riches, L., Trinidad, A.G., Fok, J.H.L., et al. (2018). The brain-penetrant clinical ATM inhibitor AZD1390 radiosensitizes and improves survival of preclinical brain tumor models. Sci. Adv. *4*, eaat1719.

16. Wang, H., Mu, X., He, H., and Zhang, X.D. (2018). Cancer Radiosensitizers. Trends Pharmacol. Sci. *39*, 24–48.

17. Loap, P., Loirat, D., Berger, F., Cao, K., Ricci, F., Jochem, A., Raizonville, L., Mosseri, V., Fourquet, A., and Kirova, Y. (2021). Combination of Olaparib with radiotherapy for triple-negative breast cancers: One-year toxicity report of the RADIOPARP Phase I trial. Int. J. Cancer *149*, 1828–1832.

18. Qin, C., Ji, Z., Zhai, E., Xu, K., Zhang, Y., Li, Q., Jing, H., Wang, X., and Song, X. (2022). PARP inhibitor olaparib enhances the efficacy of radiotherapy on XRCC2-deficient colorectal cancer cells. Cell Death Dis. *13*, 505.

19. Fan, Y., Fan, H., Quan, Z., and Wu, X. (2021). Ionizing Radiation Combined with PARP1 Inhibitor Reduces Radioresistance in Prostate Cancer with RB1/TP53 Loss. Cancer Invest. *39*, 423–434.

20. Schaue, D., and Mcbride, W.H. (2015). Opportunities and challenges of radiotherapy for treating cancer. Nat. Rev. Clin. Oncol. *12*, 527–540.

21. Yang, S., Wei, J., Cui, Y.H., Park, G., Shah, P., Deng, Y., Aplin, A.E., Lu, Z., Hwang, S., He, C., and He, Y.Y. (2019). m(6 A mRNA demethylase FTO regulates melanoma tumorigenicity and response to anti-PD-1 blockade. Nat. Commun. *10*, 2782.

22. Huang, H., Weng, H., and Chen, J. (2020). m(6 A Modification in Coding and Noncoding RNAs: Roles and Therapeutic Implications in Cancer. Cancer Cell *37*, 270–288.

23. Sun, T., Wu, R., and Ming, L. (2019). The role of m6A RNA methylation in cancer. Biomed. Pharmacother. *112*, 108613.

24. Dominissini, D., Moshitch-Moshkovitz, S., Schwartz, S., Salmon-Divon, M., Ungar, L., Osenberg, S., Cesarkas, K., Jacob-Hirsch, J., Amariglio, N., Kupiec, M., et al. (2012). Topology of the human and mouse m6A RNA methylomes revealed by m6A-seq. Nature *485*, 201–206.

25. Jiang, X., Liu, B., Nie, Z., Duan, L., Xiong, Q., Jin, Z., Yang, C., and Chen, Y. (2021). The role of m6A modification in the biological functions and diseases. Signal Transduct. Target. Ther. *6*, 74.

26. Schöller, E., Weichmann, F., Treiber, T., Ringle, S., Treiber, N., Flatley, A., Feederle, R., Bruckmann, A., and Meister, G. (2018). Interactions, localization, and phosphorylation of the m(6)A generating METTL3-METTL14-WTAP complex. RNA *24*, 499–512.

27. Wang, X., Feng, J., Xue, Y., Guan, Z., Zhang, D., Liu, Z., Gong, Z., Wang, Q., Huang, J., Tang, C., et al. (2016). Structural basis of N(6)-adenosine methylation by the METTL3-METTL14 complex. Nature *534*, 575–578.

28. Ping, X.L., Sun, B.F., Wang, L., Xiao, W., Yang, X., Wang, W.J., Adhikari, S., Shi, Y., Lv, Y., Chen, Y.S., et al. (2014). Mammalian WTAP is a regulatory subunit of the RNA N6-methyladenosine methyltransferase. Cell Res. *24*, 177–189.

29. Liu, J., Yue, Y., Han, D., Wang, X., Fu, Y., Zhang, L., Jia, G., Yu, M., Lu, Z., Deng, X., et al. (2014). A METTL3-METTL14 complex mediates mammalian nuclear RNA N6-adenosine methylation. Nat. Chem. Biol. *10*, 93–95.

30. Jia, G., Fu, Y., Zhao, X., Dai, Q., Zheng, G., Yang, Y., Yi, C., Lindahl, T., Pan, T., Yang, Y.G., and He, C. (2011). N6-methyladenosine in nuclear RNA is a major substrate of the obesity-associated FTO. Nat. Chem. Biol. *7*, 885–887.

31. Zheng, G., Dahl, J.A., Niu, Y., Fedorcsak, P., Huang, C.M., Li, C.J., Vågbø, C.B., Shi, Y., Wang, W.L., Song, S.H., et al. (2013). ALKBH5 is a mammalian RNA demethylase that impacts RNA metabolism and mouse fertility. Mol. Cell *49*, 18–29.

32. Wang, J.Y., and Lu, A.Q. (2021). The biological function of m6A reader YTHDF2 and its role in human disease. Cancer Cell Int. *21*, 109.

33. Kasowitz, S.D., Ma, J., Anderson, S.J., Leu, N.A., Xu, Y., Gregory, B.D., Schultz, R.M., and Wang, P.J. (2018). Nuclear m6A reader YTHDC1 regulates alternative polyadenylation and splicing during mouse oocyte development. Plos Genet. *14*, e1007412.

34. Zaccara, S., Ries, R.J., and Jaffrey, S.R. (2019). Reading, writing and erasing mRNA methylation. Nat. Rev. Mol. Cell Biol. *20*, 608–624.

35. Yu, F., Wei, J., Cui, X., Yu, C., Ni, W., Bungert, J., Wu, L., He, C., and Qian, Z. (2021). Posttranslational modification of RNA m6A demethylase ALKBH5 regulates ROS-induced DNA damage response. Nucleic Acids Res. *49*, 5779–5797.

36. Xiang, Y., Laurent, B., Hsu, C.H., Nachtergaele, S., Lu, Z., Sheng, W., Xu, C., Chen, H., Ouyang, J., Wang, S., et al. (2017). RNA m(6)A methylation regulates the ultraviolet-induced DNA damage response. Nature *543*, 573–576.

37. Zhou, J., Wan, J., Shu, X.E., Mao, Y., Liu, X.M., Yuan, X., Zhang, X., Hess, M.E., Brüning, J.C., and Qian, S.B. (2018). N(6)-Methyladenosine Guides mRNA Alternative Translation during Integrated Stress Response. Mol. Cell *69*, 636–647.e7.

38. Zhou, Z., Lv, J., Yu, H., Han, J., Yang, X., Feng, D., Wu, Q., Yuan, B., Lu, Q., and Yang, H. (2020). Mechanism of RNA modification N6-methyladenosine in human cancer. Mol. Cancer *19*, 104.

39. Taketo, K., Konno, M., Asai, A., Koseki, J., Toratani, M., Satoh, T., Doki, Y., Mori, M., Ishii, H., and Ogawa, K. (2018). The epitranscriptome m6A writer METTL3 promotes chemo- and radioresistance in pancreatic cancer cells. Int. J. Oncol. *52*, 621–629.

40. Wu, P., Fang, X., Liu, Y., Tang, Y., Wang, W., Li, X., and Fan, Y. (2021). N6-methyladenosine modification of circCUX1 confers radioresistance of hypopharyngeal squamous cell carcinoma through caspase1 pathway. Cell Death Dis. *12*, 298.

41. Visvanathan, A., Patil, V., Arora, A., Hegde, A.S., Arivazhagan, A., Santosh, V., and Somasundaram, K. (2018). Essential role of METTL3-mediated m(6)A modification in glioma stem-like cells maintenance and radioresistance. Oncogene *37*, 522–533.

42. Yang, Z., Yang, S., Cui, Y.H., Wei, J., Shah, P., Park, G., Cui, X., He, C., and He, Y.Y. (2021). METTL14 facilitates global genome repair and suppresses skin tumorigenesis. Proc. Natl. Acad. Sci. USA *118*. e2025948118.

43. Li, Z., Peng, Y., Li, J., Chen, Z., Chen, F., Tu, J., Lin, S., and Wang, H. (2020). N(6)-methyladenosine regulates glycolysis of cancer cells through PDK4. Nat. Commun. *11*, 2578.

44. Zhang, J., Bai, R., Li, M., Ye, H., Wu, C., Wang, C., Li, S., Tan, L., Mai, D., Li, G., et al. (2019). Excessive miR-25-3p maturation via N(6)-methyladenosine stimulated by cigarette smoke promotes pancreatic cancer progression. Nat. Commun. *10*, 1858.

45. Krishnakumar, R., Gamble, M.J., Frizzell, K.M., Berrocal, J.G., Kininis, M., and Kraus, W.L. (2008). Reciprocal binding of PARP-1 and histone H1 at promoters specifies transcriptional outcomes. Science *319*, 819–821.

46. Bell, N.A.W., Haynes, P.J., Brunner, K., de Oliveira, T.M., Flocco, M.M., Hoogenboom, B.W., and Molloy, J.E. (2021). Single-molecule measurements reveal that PARP1 condenses DNA by loop stabilization. Sci. Adv. *7*, eabf3641.

47. Kim, M.Y., Mauro, S., Gévry, N., Lis, J.T., and Kraus, W.L. (2004). NAD+-dependent modulation of chromatin structure and transcription by nucleosome binding properties of PARP-1. Cell *119*, 803–814.

48. Thomas, C., Ji, Y., Wu, C., Datz, H., Boyle, C., Macleod, B., Patel, S., Ampofo, M., Currie, M., Harbin, J., et al. (2019). Hit and run versus long-term activation of PARP-1 by its different domains fine-tunes nuclear processes. Proc. Natl. Acad. Sci. USA *116*, 9941–9946.

49. Saini, D.K., Kalyanaraman, V., Chisari, M., and Gautam, N. (2007). A family of G protein betagamma subunits translocate reversibly from the plasma membrane to endomembranes on receptor activation. J. Biol. Chem. *282*, 24099–24108.

50. Chen, S., Zhang, L., Li, M., Zhang, Y., Sun, M., Wang, L., Lin, J., Cui, Y., Chen, Q., Jin, C., et al. (2022). Fusobacterium nucleatum reduces METTL3-mediated m(6)A modification and contributes to colorectal cancer metastasis. Nat. Commun. *13*, 1248.

51. Yankova, E., Blackaby, W., Albertella, M., Rak, J., De Braekeleer, E., Tsagkogeorga, G., Pilka, E.S., Aspris, D., Leggate, D., Hendrick, A.G., et al. (2021). Small-molecule inhibition of METTL3 as a strategy against myeloid leukaemia. Nature *593*, 597–601.

52. Zhang, H.P., Chen, Q.K., and Xu, J.F. (2020). LPAR5 stimulates the malignant progression of non-small cell lung carcinoma by upregulating MLLT11. Eur. Rev. Med. Pharmacol. Sci. *24*, 8902–8910.

53. Minami, K., Ueda, N., Ishimoto, K., and Tsujiuchi, T. (2020). LPA5-mediated signaling induced by endothelial cells and anticancer drug regulates cellular functions of osteosarcoma cells. Exp. Cell Res. *388*, 111813.

54. Tong, C., Wang, C., Wang, Y., and Xiao, X. (2021). TNRC6C-AS1 Promotes Thyroid Cancer Progression by Upregulating LPAR5 via miR-513c-5p. Cancer Manag. Res. *13*, 6141–6155.

55. Wu, C.Y., Zheng, C., Xia, E.J., Quan, R.D., Hu, J., Zhang, X.H., and Hao, R.T. (2020). Lysophosphatidic Acid Receptor 5 (LPAR5) Plays a Significance Role in Papillary Thyroid Cancer via Phosphatidylinositol 3-Kinase/Akt/Mammalian Target of Rapamycin (mTOR) Pathway. Med. Sci. Monit. *26*, e919820.

56. Zhao, W.J., Zhu, L.L., Yang, W.Q., Xu, S.J., Chen, J., Ding, X.F., Liang, Y., and Chen, G. (2021). LPAR5 promotes thyroid carcinoma cell proliferation and migration by activating class IA PI3K catalytic subunit p110beta. Cancer Sci. *112*, 1624–1632.

57. Zhang, C., Chen, L., Peng, D., Jiang, A., He, Y., Zeng, Y., Xie, C., Zhou, H., Luo, X., Liu, H., et al. (2020). METTL3 and N6-Methyladenosine Promote Homologous Recombination-Mediated Repair of DSBs by Modulating DNA–RNA Hybrid Accumulation. Mol. Cell *79*, 425–442.e7.

58. Kraus, W.L. (2008). Transcriptional control by PARP-1: chromatin modulation, enhancer-binding, coregulation, and insulation. Curr. Opin. Cell Biol. *20*, 294–302.

59. Pascal, J.M. (2018). The comings and goings of PARP-1 in response to DNA damage. DNA Repair (Amst) *71*, 177–182.

60. Muthurajan, U.M., Hepler, M.R.D., Hieb, A.R., Clark, N.J., Kramer, M., Yao, T., and Luger, K. (2014). Automodification switches PARP-1 function from chromatin architectural protein to histone chaperone. Proc. Natl. Acad. Sci. USA *111*, 12752–12757.

61. Wacker, D.A., Ruhl, D.D., Balagamwala, E.H., Hope, K.M., Zhang, T., and Kraus, W.L. (2007). The DNA binding and catalytic domains of poly(ADP-ribose) polymerase 1 cooperate in the regulation of chromatin structure and transcription. Mol. Cell. Biol. *27*, 7475–7485.

62. Messner, S., Altmeyer, M., Zhao, H., Pozivil, A., Roschitzki, B., Gehrig, P., Rutishauser, D., Huang, D., Caflisch, A., and Hottiger, M.O. (2010). PARP1 ADP-ribosylates lysine residues of the core histone tails. Nucleic Acids Res. *38*, 6350–6362.

63. Poirier, G.G., de Murcia, G., Jongstra-Bilen, J., Niedergang, C., and Mandel, P. (1982). Poly(ADP-ribosyl)ation of polynucleosomes causes relaxation of chromatin structure. Proc. Natl. Acad. Sci. USA *79*, 3423–3427.

64. Krishnakumar, R., and Kraus, W.L. (2010). PARP-1 regulates chromatin structure and transcription through a KDM5B-dependent pathway. Mol. Cell *39*, 736–749.

65. Liu, L., He, C., Zhou, Q., Wang, G., Lv, Z., and Liu, J. (2019). Identification of key genes and pathways of thyroid cancer by integrated bioinformatics analysis. J. Cell. Physiol. *234*, 23647–23657.

66. Lee, S.C., Fujiwara, Y., Liu, J., Yue, J., Shimizu, Y., Norman, D.D., Wang, Y., Tsukahara, R., Szabo, E., Patil, R., et al. (2015). Autotaxin and LPA1 and LPA5 receptors exert disparate functions in tumor cells versus the host tissue microenvironment in melanoma invasion and metastasis. Mol. Cancer Res. *13*, 174–185.

67. Sun, X.Y., Li, H.Z., Xie, D.F., Gao, S.S., Huang, X., Guan, H., Bai, C.J., and Zhou, P.K. (2022). LPAR5 confers radioresistance to cancer cells associated with EMT activation via the ERK/Snail pathway. J. Transl. Med. *20*, 456.

68. Friedlander, M., Meniawy, T., Markman, B., Mileshkin, L., Harnett, P., Millward, M., Lundy, J., Freimund, A., Norris, C., Mu, S., et al. (2019). Pamiparib in combination with tislelizumab in patients with advanced solid tumours: results from the dose-escalation stage of a multicentre, open-label, phase 1a/b trial. Lancet Oncol. *20*, 1306–1315.

69. Minami, K., Ueda, N., Maeda, H., Ishimoto, K., Otagaki, S., and Tsujiuchi, T. (2019). Modulation of chemoresistance by lysophosphatidic acid (LPA) signaling through LPA5 in melanoma cells treated with anticancer drugs. Biochem. Biophys. Res. Commun. *517*, 359–363.